Free carrier absorption and inter-subband transitions in imperfect heterostructures

Ndebeka-Bandou, C.; Carosella, F.; Ferreira, R.; Wacker, Andreas; Bastard, G.

Published in:
Semiconductor Science and Technology

DOI:
10.1088/0268-1242/29/2/023001

2014

Document Version:
Peer reviewed version (aka post-print)

REVIEW ARTICLE

Free carrier absorption and inter-subband transitions in imperfect heterostructures

C Ndebeka-Bandou[1], F Carosella[1], R Ferreira[1], A Wacker[2] and G Bastard[1,3]

[1]Laboratoire Pierre Aigrain, Ecole Normale Supérieure, CNRS (UMR 8551), Université P. et M.Curie, Université Paris Diderot, 24 rue Lhomond F-75005 Paris, France

[2]Mathematical Physics, Lund University, Box 118, S-22100 Lund, Sweden

[3]Technical University Vienna, Photonics Institute, Gusshausstrasse 27, A-1040 Vienna, Austria

E-mail: camille.ndebeka-bandou@lpa-ens.fr, francesca.carosella@lpa-ens.fr, robson.ferreira@lpa-ens.fr, Andreas.Wacker@fysik.lu.se, gerald.bastard@lpa.ens.fr

Abstract. We present the results of a quantum mechanical modelling of the Free Carrier Absorption (FCA) in semiconductor heterolayers. Elastic and inelastic scatterers are considered with emphasis on the interface defects (optical phonons) contributions to the induced photon absorption for elastic (inelastic) scatterers. Various approaches to FCA are also presented (perturbation, Green's function technique). The connection between inter-subband absorption and FCA is thoroughly discussed. The absorption lineshape and its modification by suitable doping is presented.

This author prepared manuscript is published in
Semiconductor Science and Technology **29**, 023001 (2014)

1. Introduction

Intraband optical transitions in crystalline bulk materials are forbidden on account of the translational invariance of the crystal on the one hand and on the very small magnitude of the photon wavevector on the other hand. Both features lead to the impossibility for a free carrier to absorb or emit a photon and remain in the same band. It is therefore necessary that other agents, static scatterers (impurities) or inelastic scatterers (lattice vibrations), supply the extra wavevector to help the carrier performing the intraband transition. The Free Carrier Absorption (FCA) in non ideal bulk materials has been measured in several semiconductors and is well explained by theory. The modelling of this effect ranges from a Drude-like semi-classical approach, to quantum-mechanical perturbation theory and to Green's function formalism [1–11].

High quality, taylorable quasi two-dimensional (2D) semiconductor heterostructures are routinely obtained by modern growth techniques such as Molecular Beam Epitaxy (MBE) or Metal Organic Chemical Vapour Deposition (MOCVD)[12, 13]. The control of the layer thickness as well as the variety of different materials which can be grown make the quasi 2D heterostructures ideal candidates for opto-electronic applications. Actually, the best lasers for near infrared or visible light are Quantum Well lasers. The alternation of layers of different materials implies the loss of translation invariance along the growth direction even for perfect materials. As a result, an ideal heterostructure can absorb light due to intraband transitions provided the electric vector of the electromagnetic wave is parallel to the growth direction while for the other light polarizations no optical transitions are possible within the conduction band. Gornick and Tsui [14] reported the first experimental observation of inter- subband emission spectra in an electron gas in Si/SiO_2 structures. Soon, Ando proposed a theory of the inter-subband transitions taking into account scattering and many body effects [15]. An early proposal for a laser based on inter-subband transitions was made by Kazarinov and Suris in 1971 [16]. One had to wait for improvements in the growth techniques to get the observation of inter-subband emission in III-V materials [17–19] till, finally, the Quantum Cascade Lasers (QCL) emerged, thanks to the conjunction of mastered growth and bandgap engineering [20–22]. Besides the QCL's, a number of optical devices based on the inter-subband transitions and operating in the infrared and far infrared parts of the spectrum exist already, notably the Quantum Well Infrared Photodetectors (QWIP) (for reviews see e.g. [8, 9, 23]). Part of the QCL optimization amounts to limiting as much as possible the losses, notably for the THz emitting QCL's. Among other losses the free farrier absorption due to intra- subband as well as inter-subband transitions needs to be accurately modelled. We shall see that there does not exist any Drude-like modelling of FCA in quasi 2D structures but that one should necessarily recourse to perturbative estimates, Green's function techniques or numerical approches to account for these FCA losses.

This review is organised as follows. In part 2, we recall some salient features regarding the FCA in bulk semiconductors. In particular, we shall show the relevance of

the Drude model to explain experimental data and give representative figures of the FCA coefficient in bulk semiconductors. In part 3.1, we briefly recall the envelope function approximation that deals with heterolayers. Optical selection rules will be derived and the fundamental anisotropy of the optical response of the quasi 2D heterostructures will be highlighted. The existence of intra-subband and inter-subband transitions implies a need for generalizing FCA in the presence of subbands. In analogy with bulk materials, one of the central question in FCA type of calculations in heterolayers is the status of collision broadening and the part played by the disorder in the FCA. Should the elastic scatterers/phonons generate FCA by mixing unperturbed states or because they provide an imaginary part of the electron energies expressing the decay of any unperturbed state? It is worth stressing that there is a convenient way to modify the influence of the disorder on the optical response. It consists in applying a quantizing magnetic field parallel to the growth axis leading to a reorganization of the energy spectrum and also to a drastic reduction of the available phase space for electrons. An overview of the scattering mechanisms relevant to FCA will be presented in 3.2 with an emphasis on scatterers that are genuine to the heterolayers: the interface defects. Section 3.3 will be devoted to a discussion of the inter-subband and intra-subband absorption lineshape. Section 3.4 will present the perturbative approach to intra-subband oblique transitions (genuine FCA) and inter-subband oblique transitions in quasi 2D structures and discuss the results based on that approach. Section 3.5 will be devoted to a survey of Green's function approach to inter-subband and intra-subband optical transitions. This approach will be used to discuss the evolution from FCA in superlattices to FCA in bulk materials. The link between FCA and the effect of the inter-subband transitions on the tail of the absorption spectrum will be discussed in section 3.6. In 3.7 we will briefly discuss the transition from 2D FCA towards bulk FCA. In 3.8 we shall point out the existence of quasi selection rules that exist in imperfect heterolayers. In particular, we shall show how an ad hoc location of ionized impurities can effectively suppress impurity-related optical features. Finally, conclusions will be drawn in section 4.

2. Free Carrier Absorption in bulk semiconductor crystals

The translation invariance of crystalline materials leads to the existence of Bloch states $|n\vec{k}\rangle$ with energies $\varepsilon_{n\vec{k}}$ for the electron states, where n is the band index and $\vec{k}$ the wavevector. In the following, we restrict our considerations to cubic materials. In semiconductors doping and/or finite temperature induce a finite population in the conduction band. At thermal equilibrium and due to the low carrier concentration (compared to metals), it is fair to approximate the dispersion relations by parabola around the conduction band minimum. In the following we shall use an isotropic dispersion for the conduction band corresponding to the effective mass m^*, a situation approximately realized in several technologically important materials like GaAs. The generalization to anisotropic bands, as relevant for the conduction band mimina of Si, is straightforward. At this point it is easily proven that the intraband transition $|c\vec{k}\rangle \rightarrow$

$|c\vec{k'}\rangle$ with the simultaneous absorption of a photon $\left(\omega = \frac{\hbar}{2m^*}(k'^2 - k^2)\ ,\ \vec{q} = \vec{k'} - \vec{k}\right)$ is impossible because both energy and wavevector conservations cannot be satisfied. The departure from ideality of any crystal breaks the translation invariance and allows such an oblique (in $\vec{k}$ space) transition. The simplest way to account for these oblique transitions is to perform a semi-classical Drude analysis. Let us consider an electromagnetic progressive plane wave characterized by a $\vec{k}$ vector and an angular frequency ω. The associated electric field accelerates the conduction electrons which are also slowed down by a visquous friction force $-m^*\frac{\vec{v}}{\tau}$, where τ is a characteristic relaxation time. In the stationary state, both forces balance and the electron velocity becomes proportional to the electric field leading to the Ohm law:

$$\vec{J}(\omega) = \sigma(\omega)\vec{E}(\omega) \quad ; \quad \sigma(\omega) = \frac{\sigma_0}{1 - i\omega\tau} \tag{1}$$

where $\sigma_0 = \frac{n_{3D}e^2\tau}{m^*}$ is the static conductivity and n_{3D} the three dimensional (3D) electron concentration. (Note, that we use the time-dependence $J(t) \sim J(\omega)e^{-i\omega t}$ throughout the paper.) The dispersion relation of the electromagnetic wave is related to the effective relative dielectric function $\tilde{\varepsilon}(\omega)$ by:

$$k^2 = \frac{\omega^2}{c^2}\tilde{\varepsilon}(\omega) \quad ; \quad \tilde{\varepsilon}(\omega) = \varepsilon_r(\omega) + i\frac{\sigma(\omega)}{\varepsilon_0\omega} \tag{2}$$

where ε_0 is the vacuum dielectric constant and $\varepsilon_r(\omega)$ is the real part of the relative dielectric function, due e.g. to polarization effects. The absorption coefficient $\alpha(\omega)$ is equal to:

$$\alpha(\omega) = \frac{n_{3D}e^2}{n_r m^* c\varepsilon_0\omega^2\tau} \tag{3}$$

where n_r is the refractive index at the angular frequency ω and $\omega\tau \gg 1$. For GaAs-like parameters (m^*=0.07m_0, n_r=3.5, n_{3D}=10^{16} cm^{-3}, τ=1 ps) one finds $\alpha \approx 0.12$ cm^{-1} for a wavelength λ=10 μm, a value within a factor of 3 off the more reliable one obtained by solving the Boltzmann equation and evaluating the parameter τ [2]. Of course, the Drude-like approach has several limitations, both physical (e. g. lack of quantum mechanical description) but also numerical since there is no a priori knowledge of the parameter τ and a fortiori of its variations with temperature T or wavelength λ. A more microscopic approach is at stake and one can solve the Boltzmann equation with scattering probabilities deduced from the quantum matrix elements of the scattering potential. Or one attempts a perturbative approach of the disorder by expanding the carrier eigenstates to the first order in disorder. This method will be detailed in section 3 when we shall discuss the FCA in quasi 2D heterostructures. Otherwise, the frequency dependent conductivity, which is the only ingredient to plug in the Maxwell equations, can be evaluated by Green's function techniques. Again this will be detailed in section 3 in quasi 2D situations. Suffice here to say that at the lowest order in the small parameter $(\omega\tau)^{-1}$ an expression similar to (3) is retrieved for bulk materials, with the important improvement that the phenomenological parameter τ is now a well defined quantity that can be precisely calculated in terms of the band parameters, temperature, elastic scatterers and phonons present in the material.

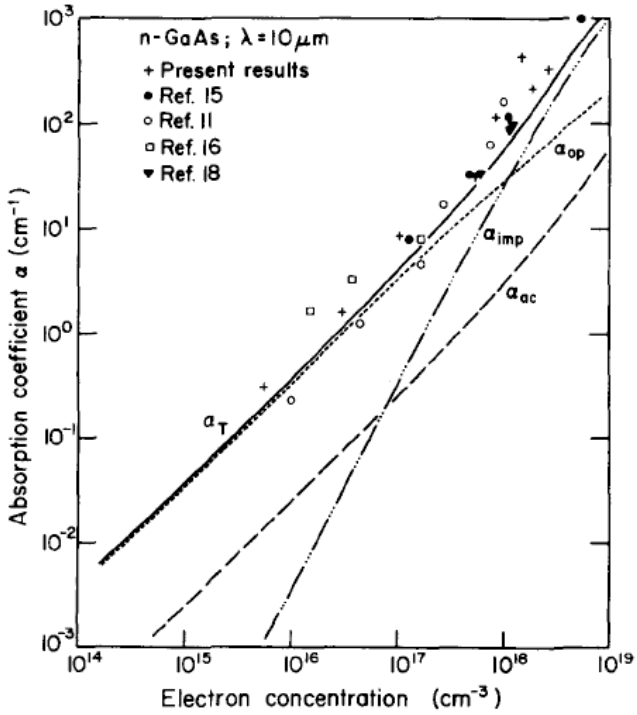

Figure 1. Theoretical and experimental values of the absorption coefficient as a function of electron concentration in GaAs at room temperature. Walukiewicz *et al* . Reprinted with permission from [2]. Copyright 1979, American Institute of Physics.

Figure 1 shows a representative example of FCA in bulk semiconductors. In figure 1 the material is GaAs and T=300 K. The absorption coefficient at λ=10 μm is plotted versus the electron concentration n_{3D}. Several scattering mechanisms have been considered: ionized impurities, electron-Longitudinal Optical (LO) phonon and electron-acoustical phonon interaction by deformation potential. Theory and experiments agree quantitatively on the absolute magnitude of FCA at λ=10 μm as well as on the wavelength dependence of FCA. While the Drude model predicts $\alpha_{FCA}(\lambda) \propto \lambda^2$, Boltzmann type of calculations points out a λ^p behaviour with an exponent p that is dependent on the scattering mechanism: $p \approx 2.5$ for scattering by optical phonons; $p \approx 3.5$ for ionized impurity scattering and $p \approx 1.5$ for acoustical phonon scattering [2]. Similar (but not identical) dependencies were found in other bulk materials. It might have been feared that FCA would be detrimental to interband lasers. Their usual operating wavelengths ($\lambda \leq 1$ μm) make that, despite the large electron concentrations ($n_{3D} \approx 10^{18}$ cm^{-3}) present in these interband lasers, FCA remains very small. Haug [5] reviewed FCA in bulk lasers including the photon absorption promoting a conduction electron to an upper band and concluded that FCA was so small that it becomes irrelevant to the lasing action in bulk semiconductors.

3. Intra- and inter-subband absorption in quantum structures

3.1. Envelope function approach in quasi two-dimensional heterostructures

Advanced growth techniques such as MBE or MOCVD have made possible the growth of nanometer thin layers with (relatively) well controlled interfaces (for a recent review see e.g. [12, 13]). With this synthesis breakthrough, all sorts of semiconductor heterostructures are within reach, ranging from single quantum well structures with only two interfaces, periodic sequences (called superlattices) up to the most elaborate ones: the Quantum Cascade Laser consisting of series of wells and barriers with different thickness repeated hundreds of times.

A number of theoretical techniques have been employed to calculate the electronic structure of these man made materials. Here, we restrict our considerations to the Envelope Function Approximation [24]. In its simpler version (one band), the envelope functions F_c are the solutions of the effective Hamiltonian H_{eff} [25]:

$$\left[p_z\left(\frac{1}{2m^*(z)}\right)p_z + \frac{p_x^2+p_y^2}{2m^*(z)} + V_{conf}(z) + V_{dis}(\vec{r})\right]F_c(\vec{r}) = \varepsilon F_c(\vec{r}) \tag{4}$$

where $m^*(z)$ is the conduction band effective mass that has become position dependent because there are different layers in the heterostructure along the z growth direction. $V_{conf}(z)$ is the position dependent conduction band edge. Both $V_{conf}(z)$ and $m^*(z)$ display sudden changes at the interfaces between different layers. The term V_{dis} accounts for impurities, alloy fluctuations like in bulk materials. It also comprises a contribution genuine to heterolayers: the interface defects. Finally, electrons interact with phonons. In polar materials, the Fröhlich interaction between the electrons and the LO phonons is written:

$$\begin{aligned} H_{e-ph} &= \sum_{\vec{Q},Q_z} v(\vec{Q},Q_z)e^{-i\vec{Q}.\vec{\rho}}e^{-iQ_z z}a^\dagger_{\vec{Q},Q_z} + v^*(\vec{Q},Q_z)e^{i\vec{Q}.\vec{\rho}}e^{iQ_z z}a_{\vec{Q},Q_z} \\ v(\vec{Q},Q_z) &= \frac{iC_F}{\sqrt{Q^2+Q_z^2}} \quad ; \quad C_F = e\sqrt{\frac{\hbar}{2\varepsilon_0\varepsilon_r(\infty)\omega_{LO}}\left(\omega_{LO}^2-\omega_{TO}^2\right)} \end{aligned} \tag{5}$$

In (5) $\vec{\rho} = (x, y)$ and bulk-like phonons are assumed. $\vec{Q} = (Q_x, Q_y)$; ω_{LO}, ω_{TO} are the angular frequencies of longitudinal and transverse optical phonons respectively and $\varepsilon_r(\infty)$ is the high frequency dielectric permittivity. A similar expression holds for longitudinal acoustical phonons; for details see [26].

The size quantization allows the tailoring of the energy levels and, thus, of the absorption/emission line position. One finds readily that the infrared (IR), far IR and even THz parts of the electromagnetic spectrum can be covered by a suitable design of the layer thicknesses. These features are at the heart of the QWIP and QCL devices. Both QWIP and QCL have already received a considerable attention and the reader is referred e.g. to [9, 21–23] for suitable reviews. As an example of the taylorability of the QCL emission energy, we show in figure 2 the calculated energy levels of a 10 nm/2 nm/L_2 biased double quantum well (DQW) subjected to a longitudinal

static electric field $\vec{F}//z$ with F=12 kV/cm varying the well thickness L_2 and keeping the intermediate barrier thickness L_b=2 nm constant. The material parameters are appropriate to the (Ga,In)As/Ga(As,Sb) lattice-matched heterolayers where each alloy is treated in the Virtual Crystal Approximation i.e. a conduction band discontinuity equal to 360 meV and an electron effective mass m^*_w=0.043m_0 in the well material (Ga,In)As and m^*_b=0.045m_0 in the barrier material Ga(As,Sb). The energy spectrum for the bound states is organized in doublets corresponding to the hybridization between the single well solutions. We see in figure 2 the familiar anticrossing schemes where a level (E_1, E_3) essentially localized in the 10 nm well and with a constant energy versus L_2 anti-crosses levels with decreasing energy versus L_2. This happens near L_2=10 nm where the eigenstates (χ_3, χ_4) and (χ_1, χ_2) are delocalised over the two wells. (Due to the curvatures of the lines before crossing, the minimal separation in energy is slightly shifted to higher values of L_2.) At large L_2 the spatial localization of the eigenstates increases with increasing well thickness.

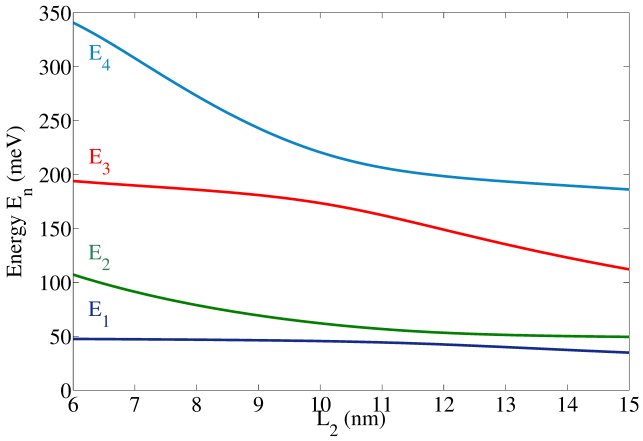

Figure 2. Calculated energy levels of (Ga,In)As/Ga(As,Sb) 10 nm/2 nm/L_2 DQW for a fixed electric field F. The parameters of the calculation are: m^*_w=0.043m_0, m^*_b=0.045m_0, V_b=360 meV. F=12 kV/cm.

In the presence of a plane progressive wave propagating along the $\vec{q}$ direction with electric vector $\vec{E} = \vec{\varepsilon} e^{i(\vec{q}.\vec{r}-\omega t)}$ where $\vec{\varepsilon}$ is the polarization vector, one should at the dipole approximation add a term

$$H_{light} = \frac{e}{i\omega}\vec{\varepsilon}.\frac{1}{2}\left[\frac{1}{m^*(z)}\vec{p} + \vec{p}\frac{1}{m^*(z)}\right] e^{-i\omega t} \quad ; \quad \vec{\varepsilon}.\vec{q} = 0 \tag{6}$$

to the electron effective Hamiltonian H_{eff}. An ideal heterostructure is translation invariant in the (x, y) plane but has lost its translation invariance along the growth z axis. As a result, there will be no light absorption for the polarization vector laying in the (x, y) plane whereas an electromagnetic wave propagating in the layer plane with its polarization vector along z may induce electronic inter-subband transitions. In fact, the (envelope) eigenstates of H_{eff} for an ideal heterostructures can be written:

$$\langle \vec{r} \mid n\vec{k} \rangle = \chi_n(z)\frac{e^{i\vec{k}.\vec{\rho}}}{\sqrt{S}} \tag{7}$$

where $\vec{k} = (k_x, k_y)$, S is the sample area and the corresponding eigenenergies are $\varepsilon_{nk} = E_n + \frac{\hbar^2 k^2}{2m^*}$. The index n is discrete (continuous) for the bound (extended) states $\chi_n(z)$ of the z motion. With this, we find readily the momentum matrix elements:

$$\langle n'\vec{k'} \mid \vec{\varepsilon}.\vec{p} \mid n\vec{k} \rangle = \delta_{\vec{k},\vec{k'}} \left[\langle n'|p_z|n\rangle \varepsilon_z + \hbar\vec{\varepsilon}.\vec{k}\delta_{n,n'} \right] \tag{8}$$

Note that intra-subband transitions (n'=n) remain energetically forbidden in any polarization. However, elastic scatterers and phonons will allow these intra-subband transitions.

The notion of FCA has to be redefined in quasi 2D heterostructures since the direct analogy with FCA in bulk materials would be restricted to the intra-subband absorption. Actually, for a given photon energy, say the lasing energy in a QCL, besides an intra-subband absorption, one may also find inter-subband transitions. Hence, FCA in quasi 2D structures must comprise both types of transitions. It is in fact mandatory to include the inter-subband oblique transitions if one wants to describe the FCA evolution from a quasi 2D structures to that in a bulk material (see section 3.5) [27].

One of the most powerful tools of investigation of quasi-2D materials is the application of a very strong magnetic field parallel to the growth axis. The continuous in-plane dispersion becomes replaced by a fan of discrete Landau levels which are equidistant for parabolic dispersion. In fact, for an ideal heterostructure H_{eff} becomes:

$$\left[p_z \left(\frac{1}{2m^*(z)} \right) p_z + \frac{p_x^2 + (p_y + eBx)^2}{2m^*(z)} + V_{conf}(z) \right] F_c(\vec{r}) = \varepsilon F_c(\vec{r}) \tag{9}$$

where the transverse gauge ($\vec{A} = (0, Bx, 0)$) has been used. The solutions of (9) are:

$$F_c(\vec{r}) = \langle \vec{r}|n, p, k_y\rangle = \chi_n^{(p)}(z) \frac{e^{ik_y y}}{\sqrt{L_y}} \, \varphi_p(x + \lambda^2 k_y) \quad ; \quad \lambda = \sqrt{\frac{\hbar}{eB}} \tag{10}$$

where φ_p is the p^{th} Hermite function:

$$\varphi_p(x) = \frac{1}{\sqrt{2^p p! \lambda \sqrt{\pi}}} \, \exp\left(-\frac{(x + \lambda^2 k_y)^2}{2\lambda^2} \right) H_p\left(\frac{(x + \lambda^2 k_y)}{\lambda} \right)$$

$$H_p(x) = (-1)^p e^{x^2} \frac{d^p}{dx^p}(e^{-x^2}) \tag{11}$$

Note that the eigenenergies do not depend on k_y, which leads to a macroscopic degeneracy of the eigenenergies ε_{np}. The z dependent eigenfunctions $\chi_n^{(p)}(z)$ depend on the Landau level index p because the effective mass $m^*(z)$ is position dependent. But this dependence is very weak for tightly bound states that are usually the ones involved in the lasing action of QCL's. One of the most striking consequences of the Landau quantization is the modulation of inter-subband scattering [28]. For instance, in absence of magnetic field, elastic scatterings allow inter-subband transitions for any initial in-plane wavevector. On the contrary, when $B \neq 0$ an electron initially in the state $|n, p, k_y\rangle$ can undergo an elastic scattering to $|n', p', k'_y\rangle$ only if the energies of the two states coincide, which is usually impossible. When this is made possible by an accidental degeneracy between ε_{np} and $\varepsilon_{n'p'}$ the evaluation of the scattering rate requires going beyond the Born approximation [3, 15, 29].

3.2. Scattering mechanisms in quasi two-dimensional heterostructures

While the scatterers in quasi 2D structures may be the same ionized impurities as in bulk materials, the breakdown of translation invariance along z implies important modifications of their scattering efficiency together with a marked dependence upon the impurity location. An important difference between bulk and quasi 2D materials is the existence of a novel scattering mechanism that is genuine to heterolayers: the interface defect scattering. The efficiency of alloy scattering is also modified in quasi 2D materials since it can be very much weakened if the alloy scattering occurs in the barrier-acting materials. On the other hand, apart from the existence of interface phonon modes, the scattering by phonons in bulk and quasi 2D materials are qualitatively the same. They however quantitatively differ.

3.2.1. Impurities While it is clear that the unit cell that hosts an impurity is irrelevant in a bulk crystal, it becomes very important to specify the relative position of the impurities and the initial and/or final state in heterostructures. Typically, the impurity scattering will be efficient if the impurity location along the z axis is close from a maximum of the square modulus of the envelope functions for the initial or final state, while it will be negligible if the impurity is far away from the states involved in the transition. We illustrate this feature by displaying the variations of the inter-subband matrix element of the Coulomb potential created by one impurity $\langle 2\vec{k}|\frac{-e^2}{4\pi\varepsilon_0\varepsilon_r\sqrt{(\vec{\rho}-\vec{\rho_j})^2+(z-z_i)^2}}|1\vec{k'}\rangle$ versus z_i for the DQW structure of figure 2 and a fixed $\vec{q}=\vec{k'}-\vec{k}$ where $(\vec{\rho_j}, z_i)$ is the impurity location. One finds readily:

$$\langle 2\vec{k}|\frac{-e^2}{4\pi\varepsilon_0\varepsilon_r\sqrt{(\vec{\rho}-\vec{\rho_j})^2+(z-z_i)^2}}|1\vec{k'}\rangle = \frac{-e^2}{2\varepsilon_0\varepsilon_r S}\times\frac{e^{-i\vec{q}.\vec{\rho_j}}\langle 2|e^{-q|z-z_i|}|1\rangle}{q} \quad (12)$$

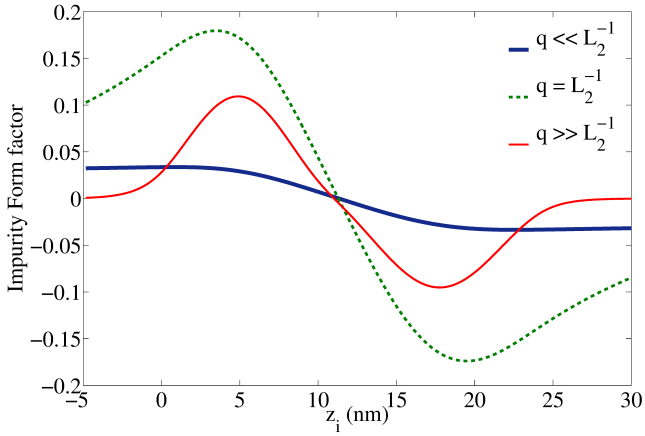

Figure 3. The impurity form factor $\langle 1|e^{-q|z-z_i|}|2\rangle$ is plotted versus the impurity location z_i along the growth axis for several q values in the case of the double quantum well structure 10/2/12 nm of figure 2 with E_1=46.8 meV and E_2=56.3 meV.

Thus, it is enough to display in figure 3 the z_i dependence of the impurity form factor $\langle 2|e^{-q|z-z_i|}|1\rangle$ for several values of q since the in-plane impurity location $\vec{\rho_j}$ disappears in a Born type calculation where the scatterers are assumed uncorrelated. As a matter of fact, when there are many impurities distributed at random, the different phase factors $e^{-i\vec{q}.\vec{\rho_j}}$ oscillate and as a result the squared modulus of the sum of the impurity matrix elements reduces to N times that of a single impurity. Hence, the in-plane location is not so important as expected from unperturbed eigenstates that are uniformly distributed in the layer plane. On the reverse, the impurity location along the growth axis does matter since the modulus of the matrix element can be very small (impurity far in the right hand side or left hand side barriers) or, as shown in figure 3, may reach a maximum when z_i is near the maximum of either $|\chi_1|^2$ or $|\chi_2|^2$. These considerations are of relevance when the optimisation of a structure is searched.

The Coulombic potentials are screened by the free carriers (see e.g. [3] for a thorough discussion of screening effects in quasi 2D heterostructures). But in QCL structures the carrier concentration is very low (typically 4×10^{10} cm^{-2} for THz QCL's) and the screening is quite weak. Low carrier concentrations ensure the validity of the Debye-Huckel approximation, in particular when T is not too low. It has been pointed out [30] that for extended structures such as superlattices or QCLs, 3D Debye-Huckel screening might be a better approximation to the actual screened potential than the 2D Debye-Huckel screening. In such a 3D case, the screened coulombic potential created by a donor located at $(\vec{\rho_j}, z_i)$ admits the Fourier Bessel expansion:

$$V(\vec{\rho}, z) = \frac{-e^2}{2\varepsilon_0\varepsilon_r S}\sum_{\vec{Q}}\frac{e^{i\vec{Q}.(\vec{\rho}-\vec{\rho_j})}}{\sqrt{Q^2+Q_s^2}}\; e^{-|z-z_i|\sqrt{Q^2+Q_s^2}} \tag{13}$$

where Q_s is the classical wavevector:

$$Q_s = \sqrt{\frac{e^2 n_{3D}}{\varepsilon_0\varepsilon_r k_B T}} \tag{14}$$

where n_{3D} is the equivalent 3D carrier concentration. For n_{3D}=10^{15} cm^{-3}, $T \approx 100$ K and ε_r=12.4, one finds $Q_s^{-1} \approx 70$ nm, i.e. a distance much larger than a typical effective Bohr radius. Thus, impurities will be little screened and their bound states will survive with a substantial binding.

3.2.2. Interface roughness A scattering mechanism genuine to heterolayers is the interface roughness. By this it is meant that the interface separating two materials deviates from a plane. Note that we have implicitly assumed working in the envelope function formalism. In a more microscopic approach the interface, even ideal, does not reduce to a plane but to a collection of ideally placed atoms. Because little is known on the formation of interfaces, people have tried to use interface models that are as simple as possible [31, 32]. A very popular model is the one that relates interface roughness potential to correlated in-plane fluctuations of the position of the interface. This model is detailed e.g. in [3] and [15]. Let $\Delta(\vec{\rho})$ be the deviation of the interface from a plane.

The nominal hetero-interface is at $z{=}z_0$ and the barrier height is V_b. Hence, an electron experiences a potential energy:

$$\begin{aligned} V(\vec{\rho},z) &= V_b Y(z-z_0+\Delta(\vec{\rho})) \\ &= V_b Y(z-z_0) + V_b\left[Y(z-z_0+\Delta(\vec{\rho}))-Y(z-z_0)\right] \end{aligned} \tag{15}$$

where $Y(x)$ is the step function: $Y(x)=1$ if $x>0$; $Y(x)=0$ if $x<0$. The potential energy has been written as the sum of an unperturbed contribution due to the ideal interface and a perturbation $\delta V_{def} = V_b\left[Y(z-z_0+\Delta(\vec{\rho}))-Y(z-z_0)\right]$. The matrix element between $|n\vec{k}\rangle$ and $|n'\vec{k'}\rangle$ of this perturbation is equal to:

$$\begin{aligned} \langle n\vec{k}|\delta V_{def}|n'\vec{k'}\rangle = \frac{V_b}{S}\int d^2\rho e^{i(\vec{k'}-\vec{k}).\vec{\rho}} \\ \times \int dz \chi_n^*(z)\chi_{n'}(z)\left[Y(z-z_0+\Delta(\vec{\rho}))-Y(z-z_0)\right] \end{aligned} \tag{16}$$

If one assumes that Δ remains small compared to the penetration length of the unperturbed envelope functions in the barrier, we get:

$$\begin{aligned} \langle n\vec{k}|\delta V_{def}|n'\vec{k'}\rangle &= \frac{V_b}{S}\int d^2\rho e^{i(\vec{k'}-\vec{k}).\vec{\rho}}\int_{z_0-\Delta(\vec{\rho})}^{z_0} dz\chi_n^*(z)\chi_{n'}(z) \\ &\approx \frac{V_b}{S}\chi_n^*(z_0)\chi_{n'}(z_0)\int d^2\rho e^{i(\vec{k'}-\vec{k}).\vec{\rho}}\Delta(\vec{\rho}) \end{aligned} \tag{17}$$

The fluctuations $\Delta(\vec{\rho})$ have a zero average. Hence, there is no energy shifts to the first order in Δ. When calculating scattering rates one should average the squared modulus of the matrix elements:

$$\begin{aligned} \langle\ \left|\langle n\vec{k}|\delta V_{def}|n'\vec{k'}\rangle\right|^2\ \rangle_{av} = \frac{V_b^2}{S^2}|\chi_n^*(z_0)|^2|\chi_{n'}(z_0)|^2 \\ \times\int\int d^2\rho d^2\rho' e^{i(\vec{k'}-\vec{k}).(\vec{\rho}-\vec{\rho'})}\langle\Delta(\vec{\rho})\Delta(\vec{\rho'})\rangle_{av} \end{aligned} \tag{18}$$

In this approach of the interface roughness the correlation function $\langle\Delta(\vec{\rho})\Delta(\vec{\rho'})\rangle_{av}$ plays the central role. Very often [3], one assumes it is a Gaussian function of $|\vec{\rho}-\vec{\rho'}|$:

$$\langle\Delta(\vec{\rho})\Delta(\vec{\rho'})\rangle_{av} = \Delta^2\exp\left(-\frac{(\vec{\rho}-\vec{\rho'})^2}{\Lambda^2}\right) \tag{19}$$

Alternatively, one can use an expontential distribution

$$\langle\Delta(\vec{\rho})\Delta(\vec{\rho'})\rangle_{av} = \Delta'^2\exp\left(-\frac{|\vec{\rho}-\vec{\rho'}|}{\Lambda'}\right) \tag{20}$$

which appears to fit better with experimental data [33–35]. Choosing $\Lambda' = \Lambda/\sqrt{6}$ and $\Delta' = \sqrt{3}\Delta$ provides identical Fourier transforms around $q=0$.‡

Finally, one gets the averaged matrix element:

$$\langle\ \left|\langle n\vec{k}|\delta V_{def}|n'\vec{k'}\rangle\right|^2\ \rangle_{av} = \frac{V_b^2}{S}|\chi_n^*(z_0)|^2|\chi_{n'}(z_0)|^2\Delta^2\pi\Lambda^2\exp\left(-\frac{(\vec{k'}-\vec{k})^2\Lambda^2}{4}\right) \tag{21}$$

where the statistical coefficients Δ and Λ are usually treated as fitting parameters. Note that we have neglected any modification of the band bending effects due to mobile and

‡ Martin Lindskog, private communication

fixed charges associated with interface fluctuations. Ando *et al* have discussed these modifications in details in particular in the Si/SiO_2 case. In QCL structures we expect these modifications to be small on account of low carrier concentrations present in these structures compared to those in Si MOSFET (a few 10^{12} cm^{-2}).

In this review, we shall use a slightly different model of interface roughness. Compared to the nominal interface $z{=}z_0$, the interface fluctuations are represented by Gaussian protrusions either from the well in the barrier or vice versa. They will be attractive (repulsive) in the former (latter) case. These protrusions are centred at the site $\vec{\rho_j}$ and are characterized by an in-plane extension σ and by a depth h_{def}: for an ideal barrier ($z \leq z_0$)/well ($z \geq z_0$) interface:

$$\begin{aligned}
&\delta V_{def}(\vec{\rho}, z) = V_b g(z) \sum_{\vec{\rho_j}} \exp\left(-\frac{(\vec{\rho} - \vec{\rho_j})^2}{2\sigma^2}\right) \\
&g(z) = +Y(z - z_0)Y(h_{def} - z + z_0) \; for \; repulsive \; defects \\
&g(z) = -Y(-z + z_0)Y(h_{def} + z - z_0) \; for \; attractive \; defects
\end{aligned} \tag{22}$$

Besides the characteristic in-plane size σ, the defects are characterized by their areal concentrations $n_{def} = \frac{N_{att}+N_{rep}}{S}$ or equivalently by the fractional coverage of the surface f_r:

$$f_r = \pi\sigma^2 n_{def} \tag{23}$$

One of the advantages of this model is that the σ and f_r parameters allow to have an immediate picture of the disorder extension. The link between the two models can be made by evaluating the averaged squared modulus of the scattering matrix element. Assuming no correlations between both the attractive and repulsive sites we get:

$$\begin{aligned}
&\langle \left|\langle n\vec{k}|\delta V_{def}|n'\vec{k'}\rangle\right|^2 \rangle_{av} = \frac{V_b^2}{S} 4\pi^2\sigma^4 \\
&\times \left(\frac{N_{rep}}{S}\left|\int_{z_0}^{z_0+h_{def}} dz \chi_n^*(z)\chi_{n'}(z)\right|^2 + \frac{N_{att}}{S}\left|\int_{z_0-h_{def}}^{z_0} dz \chi_n^*(z)\chi_{n'}(z)\right|^2\right) \\
&\times \exp\left(-(\vec{k'} - \vec{k})^2\sigma^2\right)
\end{aligned} \tag{24}$$

In the limit where the envelopes vary slowly on the scale of h_{def} we obtain:

$$\begin{aligned}
\langle\left|\langle n\vec{k}|\delta V_{def}|n'\vec{k'}\rangle\right|^2\rangle_{av} = \frac{V_b^2}{S}|\chi_n(z_0)|^2|\chi_{n'}(z_0)|^2 4\pi^2\sigma^4 h_{def}^2 \left(\frac{N_{rep}+N_{att}}{S}\right) \\
\times \exp\left(-(\vec{k'} - \vec{k})^2\sigma^2\right)
\end{aligned} \tag{25}$$

Comparing (21) and (25) we get:

$$\Lambda = 2\sigma \quad ; \quad \Delta = h_{def}\sqrt{f_r} \tag{26}$$

Another advantage of writing δV_{def} as a random muffin tin potential lays in its capability to handle bound states associated with the interface defects. These bound states are however shallow (of the order of 1 meV) in GaAs/(Ga,Al)As heterostructures because h_{def} is small (one monolayer) and very often the wavefunctions are small at the interfaces. The interface roughness affects the various subbands differently since

the amplitudes of the wavefunctions at the interfaces markedly depend on the subband index. We show in figure 4 the potential energy landscape for the in-plane motion in a GaAs/(Ga,Al)As DQW for the E_1 subband. To draw figure 4 the 3D defect potential $\delta V_{def}(\vec{\rho}, z)$ is averaged over the χ_1 state:

$$\begin{aligned}\delta V_{def,2D}(\vec{\rho}) &= \int_{-\infty}^{+\infty} dz \chi_1^2(z) \delta V_{def}(\vec{\rho}, z) \\ &= -V_b \int_{z_0}^{z_0+h_{def}} dz \chi_1^2(z) \sum_{\vec{\rho}_{att}} \exp\left(-\frac{(\vec{\rho}-\vec{\rho}_{att})^2}{2\sigma^2}\right) \\ &+ V_b \int_{z_0-h_{def}}^{z_0} dz \chi_1^2(z) \sum_{\vec{\rho}_{rep}} \exp\left(-\frac{(\vec{\rho}-\vec{\rho}_{rep})^2}{2\sigma^2}\right) \end{aligned} \quad (27)$$

The attractive and repulsive sites are random 2D vectors and figure 4 corresponds to one particular realisation of the interface disorder. Note that any calculated property associated with the interface roughness has to involve an average over the disorder realisation; in practice each property is calculated for a large number of different choices for the repulsive and attractive sites.

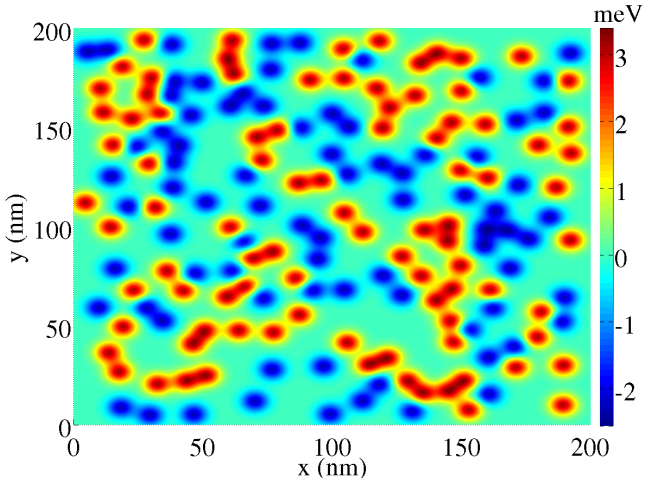

Figure 4. Potential energy landscape for the in-plane motion of an electron in a 7/2/10 nm GaAs/$Ga_{0.75}Al_{0.25}As$ DQW. The barrier height is 217.5 meV. The defect parameters are f_r=0.3, σ=3.6 nm and h_{def} = 0.283 nm. The interface defects are placed on the second interface starting from the left.

To illustrate the shallowness of the bound states created by interface defects in the GaAs/GaAlAs system we show in figure 5 the calculated in-plane squared envelope functions of several states (bound and unbound) associated with the E_2 subband of a 9/2/3nm GaAs/$Ga_{0.75}Al_{0.25}As$ DQW. In these calculations the inter-subband scattering is neglected and attractive potentials bind states for the in-plane motion below each of the E_n edges. The numerical diagonalization is undertaken in a 200 nm $\times$ 200 nm box using a basis of periodic plane waves. Taking the inter-subband contribution into account transforms these discrete states into resonances. These resonances may be long lived (as well as the trapping of carriers onto the defects effective) if the binding energies

are larger than the broadening due to escape. This is barely true for interface defects in figure 5 but is well obeyed for donor impurities , as discussed later. Interface roughness is expected to play a more important part in systems where the anions are different, e.g. InAs/(Ga,Al)Sb or (Ga,In)As/Ga(As,Sb). This is because the growth always ends up with a group V plane. Hence, in a AlSb/InAs/AlSb single QW the barrier growth stops at a Sb plane. Then, the InAs growth proceeds letting an InSb double layer in between the AlSb and InAs layers. The InAs growth ends by an As plane. The growth of the second AlSb barrier leaves an AlAs double layer between the InAs and AlSb layers. The atomic structures of these double layers are not very well known and a fortiori the structure of an interface defect is certainly much more complex than in the systems with common group V elements and should probably have a deeper extension along the z axis than one monolayer as found in GaAs/(Ga,Al)As.

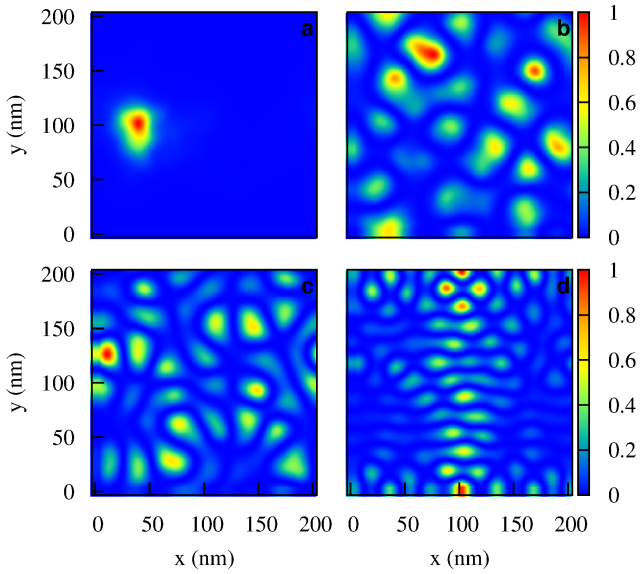

Figure 5. Normalized in-plane squared envelope functions of several states with energy E and associated with the E_2 subband of a 9/2/3 nm GaAs/$Ga_{0.75}Al_{0.25}As$ DQW. The barrier height is 217.5 meV. The inter-subband scattering is neglected. Panel a: E=E_2-1.3 meV (first bound state). Panel b: E=E_2+5 meV. Panel c: E=E_2+10 meV. Panel d: E=E_2+20 meV.

3.2.3. Alloy scattering The effect of alloy scattering is much affected by the size quantization due to the unequal spatial distribution of the eigenstates among the different layers. Clearly, alloy scattering that takes place in the barriers is for most heterolayers less prevalent than the one that takes place in the well-acting materials. The alloy scattering is due to a sum of uncorrelated short-range scatterers. For example, in $Ga_{1-x}Al_xAs$ alloys each group III site is occupied by a Ga atom with a probability x or an Al atom with a probability $1-x$. In an ideal alloy the sites are independent. Ga and Al are isovalent and the bonds between Ga and As or Al and As are very similar. So, in a first approximation, one can define a virtual crystal where all the group III element

sites are occupied by an average atom that contributes to a crystalline potential by a quantity $(1-x)V_{Ga}+xV_{Al}$. The difference δV_{alloy} between the actual and the Virtual Crystal Approximation (VCA) potential scatters the VCA Bloch waves. People are used to write:

$$\begin{aligned}\delta V_{alloy} &= \sum_{\vec{R}_{Ga}} x(V_{Ga}-V_{Al}) - \sum_{\vec{R}_{Al}}(1-x)(V_{Ga}-V_{Al}) \\ &= \Delta V \omega_0 \left[x\sum_{\vec{R}_{Ga}} \delta(\vec{r}-\vec{R}_{Ga}) - (1-x)\sum_{\vec{R}_{Al}} \delta(\vec{r}-\vec{R}_{Al}) \right] \end{aligned} \quad (28)$$

where ω_0 is the volume of the VCA unit cell and ΔV an effective strength (a fraction of an eV) which is the average of $(V_{Ga}-V_{Al})$ over this unit cell. ΔV is not very well known but it is often assumed to be related to the conduction band offset. With (28) one finds readily:

$$\begin{aligned}|\langle n\vec{k}|\delta V_{alloy}|n'\vec{k'}\rangle|^2 &= \left(\frac{\Delta V\omega_0}{S}\right)^2 \\ \times \left| x\sum_{\vec{R}_{Ga}} \chi_n(z_{Ga})\chi_{n'}(z_{Ga}) e^{i(\vec{k'}-\vec{k}).\vec{\rho}_{Ga}} - (1-x)\sum_{\vec{R}_{Al}} \chi_n(z_{Al})\chi_{n'}(z_{Al}) e^{i(\vec{k'}-\vec{k}).\vec{\rho}_{Al}} \right|^2 \end{aligned} \quad (29)$$

In (29), the summations run on the $Ga_{1-x}Al_xAs$ parts of the heterostructure. Averaging over Ga and Al sites and assuming these sites to be uncorrelated, we get:

$$\langle \left| \langle n\vec{k}|\delta V_{alloy}|n'\vec{k'}\rangle \right|^2 \rangle_{av} = \frac{x(1-x)\omega_0(\Delta V)^2}{S} \int_{Ga_{1-x}Al_xAs} dz \chi_n^2(z)\chi_{n'}^2(z) \quad (30)$$

We show in figure 6 the period length L_z dependence of $\langle M_{alloy}\rangle = \langle \left| \langle 1,\vec{k}|\delta V_{alloy}|1,\vec{k'}\rangle \right|^2 \rangle_{av}$ in a (Ga,In)As/Ga(As,Sb) single QW structure. The ΔV parameters have been assumed equal (0.6 eV) for both alloys. Unless the well is extremely narrow (such that the integrated probability in the well and in both barriers are comparable), the alloy scattering in the barrier remains negligible compared to that taking place in the well-acting material.

3.3. Inter-subband and intra-subband absorption lineshape (z polarization)

For the sake of definiteness, we shall consider in the following the z polarization in the electromagnetic field: $\vec{\varepsilon}//\hat{z}$. For an ideal heterostructure, there is no intra-subband transition while the inter-subband transition is allowed and gives rise for parabolic in-plane dispersion relations to a delta-like absorption. In the following, we shall present results in terms of absorption coefficient (like in 3D materials). To do so, we shall first evaluate the energy loss rate of electrons $P(\omega)$ by using the Fermi Golden Rule to handle the interaction between matter and electromagnetic (e.m.) wave and relate this $P(\omega)$ to the absorption coefficient $\alpha(\omega)$ by assuming that light is uniform over the N_p periods (one period length L_z) of the structure. Under such an assumption, α and P are related by:

$$\alpha(\omega) = \frac{2P(\omega)}{\varepsilon_0 c n_r E_{em}^2 L_z S} \quad (31)$$

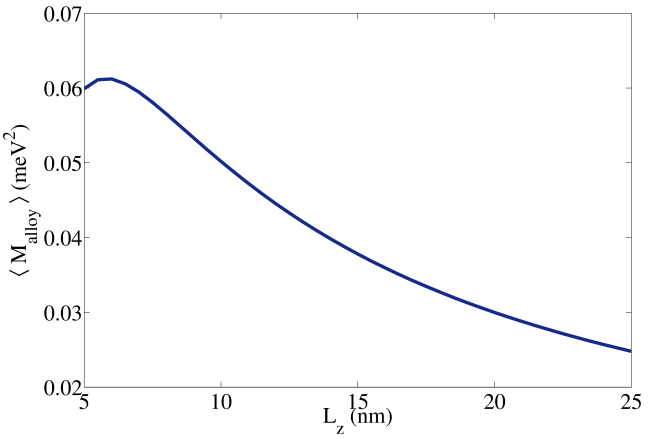

Figure 6. L_z dependence of $\langle M_{alloy}\rangle = \langle \left| \langle 1, \vec{k}|\delta V_{alloy}|1, \vec{k'}\rangle \right|^2 \rangle_{av}$ in a (Ga,In)As/Ga(As,Sb) single QW structure. m_w^*=0.043m_0, m_b^*=0.04m_0, V_b=360 meV.

where E_{em} is the electric field strength of the em wave. **Note that eq.(31) is established under the assumption of weak absorption (in the evaluation of the flux of the Poynting vector, plane waves for the e.m. fields are used). As expressed in terms of the real (k_1) and imaginary (k_2) parts of the wavevector of the e.m. waves, this means that $k_1 \gg k_2$. But if the weak absorption limit is valid $k_1 \approx \frac{n_r\omega}{c}$, where n_r is the refractive index. On the other hand, k_2 is linked to the absorption coefficient $\alpha(\omega)$ by $k_2 = \frac{\alpha(\omega)}{2}$. As long as $k_1/k_2 \gg 10$ the weak absorption limit is well justified. We will show in figures 9 and 14, taken as representative examples, together with $\alpha(\omega)$ the variations of k_1/k_2 versus the photon energy $\hbar\omega$. We shall see that the weak absorption limit is well followed, except in the immediate vicinity of resonances where the perturbative approches used become unreliable and must be replaced by more refined or even exat approches. The latter will be handled in sections 3.5 and 3.6.**

For an ideal heterostructure both P_{intra} and α_{intra} vanish for intra-subband transitions while:

$$\alpha_{inter}^{1\to 2}(\omega) = \frac{\pi e^2}{m^{*2}\omega\varepsilon_0 c n_r L_z}(n_1 - n_2)|\langle 1|p_z|2\rangle|^2\delta(E_2 - E_1 - \hbar\omega) \tag{32}$$

where n_1 and n_2 are the 2D concentrations of electrons in the subband 1 and 2 respectively and where we have neglected the z dependence of the effective mass. By using $\frac{i\hbar p_z}{m^*} = \left[z, \frac{p^2}{2m^*}\right]$, (32) can be written in term of the inter-subband dipole operator:

$$\alpha_{inter}^{1\to 2}(\omega) = \frac{\pi e^2\omega}{\varepsilon_0 c n_r L_z}(n_1 - n_2)|\langle 1|z|2\rangle|^2\delta(E_2 - E_1 - \hbar\omega) \tag{33}$$

Here, we used $E_2 - E_1 = \hbar\omega$ which is justified due to the delta function. Alternatively, one obtains this expression if one approximates the coupling to the electromagnetic field via the $\vec{E}\cdot\hat{d}$ term (where $\hat{d}$ is the electric dipole moment), while we used $\vec{A}\cdot\hat{p}$-coupling

in the Fermi's golden rule treatment above. Taking broadening effects into account empirically transforms the delta function into a Lorentzian:

$$\alpha_{inter}^{1\to 2}(\omega) = \frac{e^2\omega}{\varepsilon_0 c n_r L_z}(n_1 - n_2)|\langle 1|z|2\rangle|^2 \frac{\Gamma}{\Gamma^2 + (E_2 - E_1 - \hbar\omega)^2} \tag{34}$$

Without the delta-function, the ω-dependence of the prefactor provides different behavior, depending on the coupling to the electromagnetic field used. At this stage, we do not have a convincing argument, which one is better, but obviously, one has to be careful if $E_2 - E_1$ and $\hbar\omega$ strongly differ. For Γ=2 meV, $n_1 - n_2$=10^{11} cm^{-2}, n_r=3.5, $|\langle 1|z|2\rangle|$=2.2 nm, L_z=30 nm, $\hbar\omega$=100 meV, we find at resonance: $\alpha_{inter}^{1\to 2} \approx 2.3\times 10^3$ cm^{-1}. Thus, inter-subband absorption is a strongly allowed transition. Note that the high energy tail of $\alpha_{inter}^{1\to 2}$ ($\hbar\omega - E_2 + E_1 \gg \Gamma$) varies like $\frac{\omega}{(\hbar\omega - E_2 + E_1)^2}$ while the absorption coefficient varies like ω at very low frequency.

There are two difficulties with (34). The first one is the incorrect identification of the absorption peak with the single particle energy difference $E_2 - E_1$. This difference comprises the level renormalisations due to scattering and the depolarization and exciton shifts and increases with $n_1 - n_2$. The latter one amounts to a few meV's when $n_1 - n_2$ is a few 10^{11} cm^{-2} in the GaAs/GaAlAs heterostructures [18]. Secondly, the status of the broadening parameter Γ in (34) is unclear since there is no handling of the real scattering mechanisms, in particular of their subband dependence. Frequently one applys state-dependent semiclassical scattering rates, see, e.g., [36], where collisional broadening was included. However, this may be problematic far from resonance $|\hbar\omega - E_2 + E_1| \gg \Gamma$, which is of high relevance for the low-fequency absorption. In view of the strong dependence of the ionized impurity, alloy scattering and interface roughness on the location of the scatterers in the heterostructures, it is highly desirable to have a full understanding of the broadening if one wants to improve the design of the structures.

The convenient Drude approach of FCA in bulk materials fails as such in quasi 2D heterostructures because for the z polarization (by far the most used in devices such as QCLs and QWIPs) there is no balance between the electric force $-e\vec{E}_{em}$ and the friction force that lays in the xOy plane (figure 7). This implies the vanishing of the zero-frequency conductivity σ_0 in Eq. (1)§. So, any estimate of FCA absorption coefficient by means of the Drude model is likely to be off by several decades. In fact, if we were to believe (3) and apply it to THz QCL's, we would conclude that no lasing is possible.

In contrast to the bulk case, conductivity at finite frequency arises due to oscillating polarisations between the subbands in quantum well structures. This has to be treated by different models and the first non-trivial one is the perturbative approach of elastic scatterers/phonons modifications of the electronic states.

§ For quantum well structures attached to leads, such as superlattices or QCLs, a dc current is possible, but the conductivity is strongly reduced in comparison to the bulk case.

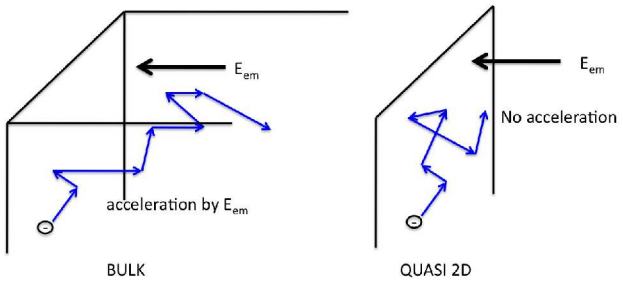

Figure 7. Comparison between the Drude model in 3D and quasi 2D situations[27].

3.4. Perturbative approach to oblique optical transitions

The idea is to get a non vanishing z current thanks to the combined actions (see figure 8) of light-matter coupling (necessarily inter-subband and vertical in $\vec{k}$ space) and elastic scatterers/phonons coupling (either intra-subband or inter-subband and oblique in $\vec{k}$ space). There is a qualitative difference between the inter-subband and intra-subband oblique transitions. In ideal structures the former are forbidden because of the in-plane translation invariance while the latter are doubly forbidden because they not only violate the in-plane translation invariance but, in addition, have a zero optical matrix element in ideal structures. One may therefore anticipate on general grounds that the intra-subband oblique transitions will be weaker than the inter-subband ones.

In the following, we develop the perturbative approach of the oblique transitions. In the examples we shall use the parameters of the DQW structure described in [27]. The well thicknesses are L_1=23.2 nm, L_2=9.8 nm and the intermediate barrier thickness is L_b=3.1 nm. The wells are GaAs and the barriers are $Ga_{0.85}Al_{0.15}As$ corresponding to a barrier height of 115 meV. The DQW supports 6 bound states for the z motion and the lasing action is supposed to occur between E_2 and E_1 ($E_2 - E_1$=16.9 meV). The aim of this example is to estimate the detrimental absorption from carriers in subband 2. There are few carriers in these structures with n_{2D}=2.17×10^{10} cm^{-2} distributed over the different subbands [37]. Hence, the depolarization shift can be neglected and the screening effects will not be very effective. We shall also present results for (Ga,In)As/Ga(As,Sb) heterostructures to highlight the part played by alloy scattering in these heterostructures.

In order to estimate the absorption, we consider the modification of eigenstates due to the disorder potential V_{dis}. Within first-order perturbation theory we find:

$$|\Psi_{n\vec{k}}\rangle = |n\vec{k}\rangle + \sum_{\vec{k'}} \frac{|n\vec{k'}\rangle\langle n\vec{k'}|V_{dis}|n\vec{k}\rangle}{\varepsilon_{n\vec{k}} - \varepsilon_{n\vec{k'}}} + \sum_{m\neq n,\vec{k'}} \frac{|m\vec{k'}\rangle\langle m\vec{k'}|V_{dis}|n\vec{k}\rangle}{\varepsilon_{n\vec{k}} - \varepsilon_{m\vec{k'}}} \qquad (35)$$

The energy loss rate $P_{ij}(\omega)$ associated with the transitions $|\Psi_{i\vec{k}}\rangle \rightarrow |\Psi_{j\vec{k'}}\rangle$ is given by:

$$P_{ij}(\omega) = \frac{\pi e^2 E_{em}^2}{\omega m^{*2}} \sum_{\vec{k},\vec{k'}} \left(f_{i\vec{k}} - f_{j\vec{k'}}\right) \left|\langle\Psi_{i\vec{k}}|p_z|\Psi_{j\vec{k'}}\rangle\right|^2 \delta(\varepsilon_{j\vec{k'}} - \varepsilon_{i\vec{k}} - \hbar\omega) \qquad (36)$$

where $f_{i\vec{k}}$, $f_{j\vec{k'}}$ are the distribution functions in the initial and final subbands

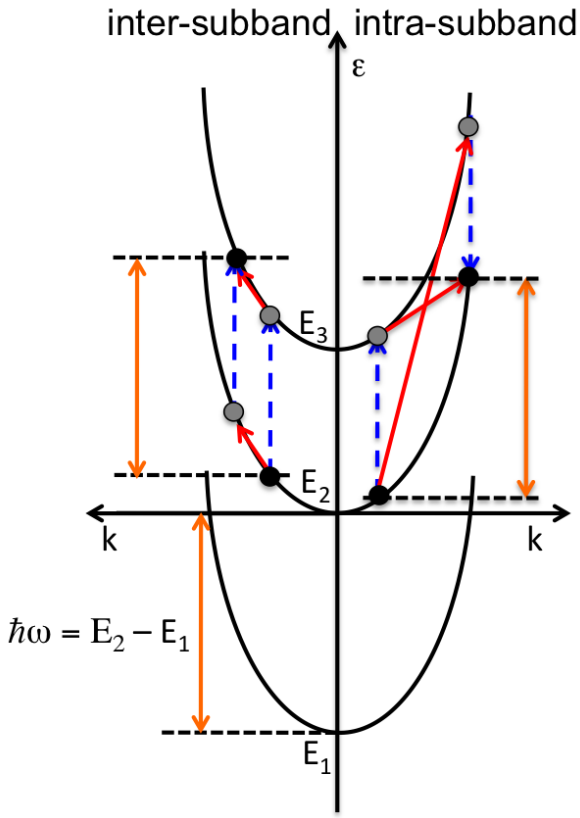

Figure 8. Energy dispersion of the E_1, E_2 and E_3 subbands. Right part: quantum mechanical path followed by an electron to undertake an intra-subband oblique transition mediated by static scatterers. Left part: quantum mechanical paths followed by an electron to undertake an inter-subband oblique transition mediated by static scatterers. Dotted lines refer to electron-photon interaction; solid lines refer to electron-scatterers interaction. Black dots are initial and final states, gray dots are virtual intermediate states[27]. In this figure, the oblique transitions occur at the same energy as the designed lasing energy $E_2 - E_1$.

respectively. Note that (36) takes into account the stimulated emission (second term of (36)). For an intra-subband transition ($i = j$), we find:

$$\langle \Psi_{i\vec{k}} | p_z | \Psi_{i\vec{k}'} \rangle = \sum_{m \neq i} \frac{\langle i|p_z|m\rangle \langle m\vec{k}|V_{dis}|i\vec{k}'\rangle}{E_i - E_m + \hbar\omega} + \frac{\langle i\vec{k}|V_{dis}|m\vec{k}'\rangle \langle m|p_z|i\rangle}{E_i - E_m - \hbar\omega} \tag{37}$$

where we see the interferences between the two paths shown in figure 8. We also note that the ω^{-p} law of the 3D Drude FCA will not be followed in quasi 2D materials. Instead we shall obtain a divergence any time the photon energy matches the energy distance between subbands. This divergence is artificial to the extent that collision broadening will blur the matching between $\hbar\omega$ and $E_i - E_m$. In the context of QCL this divergence indicates a poor design since $\hbar\omega$ is the laser photon energy and a resonant FCA would mean that the photon will be re-absorbed by parasitic inter-subband transitions. For

the oblique inter-subband matrix element we find:

$$\langle \Psi_{i\vec{k}}|p_z|\Psi_{j\vec{k'}}\rangle = \sum_m \frac{\langle i|p_z|m\rangle\langle m\vec{k}|V_{dis}|j\vec{k'}\rangle}{E_i - E_m + \hbar\omega} + \sum_m \frac{\langle i\vec{k}|V_{dis}|m\vec{k'}\rangle\langle m|p_z|j\rangle}{E_j - E_m - \hbar\omega} \quad (38)$$

The same comments as for (37) can be made for (38) regarding the divergences. We can note that (38) is dominated by $m = j$ in the first sum and $m = i$ in the second because inter-subband matrix elements are generally smaller than the intra-subband ones. If we restrict the summations to these dominant terms (38) reduces to:

$$\langle \Psi_{i\vec{k}}|p_z|\Psi_{j\vec{k'}}\rangle = \frac{\langle i|p_z|j\rangle}{E_i - E_j + \hbar\omega}\left(\langle j\vec{k}|V_{dis}|j\vec{k'}\rangle - \langle i\vec{k}|V_{dis}|i\vec{k'}\rangle\right) \quad (39)$$

where only the difference between the intra-subband matrix elements of the disorder potential in the initial and final subbands shows up. (39) also corresponds to a 3 subbands description of the system: the lasing action occurs between E_2 and E_1 while FCA corresponds to an oblique transitions between the E_2 and E_3 subbands. The transitions originating from E_1 are neglected because QCL's are engineered to efficiently depopulate the ground subband of the lasing transition. We note that if one could engineer disorder displaying subband independent matrix elements, there would be no FCA due to intersubband processes at all. This result is fairly general: if the initial and final subbands are identically broadened then the inter-subband absorption has no broadening [3, 38, 39]. Once the p_z matrix elements established, the Fermi Golden Rule allows computing the energy loss rate and by (31) the absorption coefficient. An average of the random positions of the scatterers has to be performed. As an example, we give in (40) the absorption coefficient for oblique $E_2 - E_3$ transitions due to the alloy scattering:

$$\begin{aligned}
\alpha^{alloy}(\omega) &= N_{eff}\frac{e^2x(1-x)(\Delta V)^2\omega_0}{m^*\hbar^2\omega\varepsilon_0 c n_r L_z} \times \frac{|\langle 2|p_z|3\rangle|^2}{(\hbar\omega - E_3 + E_2)^2}\int_{where\ alloy} dz(\chi_2^2 - \chi_3^2)^2 \\
N_{eff} = &\int d^2k\left(f_2\left(E_2 + \frac{\hbar^2k^2}{2m^*}\right) - f_3\left(E_2 + \frac{\hbar^2k^2}{2m^*} + \hbar\omega\right)\right) \\
&\times Y\left(\hbar\omega - E_3 + E_2 + \frac{\hbar^2k^2}{2m^*}\right)
\end{aligned} \quad (40)$$

In (40), the z integral runs over that part of the heterostructure where the alloy scattering takes place. For thermalized (Boltzmann) carriers in both 2 and 3 subbands, the difference between the f's gives a factor $\left(1 - e^{-\beta\hbar\omega}\right)$ to transform N_{eff} into:

$$\begin{aligned}
&N_{eff} = \left(1 - e^{-\beta\hbar\omega}\right)2\pi n_2 \\
&\times \left(Y(\hbar\omega - E_3 + E_2) + Y(-\hbar\omega + E_3 - E_2)\exp\left(-\beta(-\hbar\omega + E_3 - E_2)\right)\right)
\end{aligned} \quad (41)$$

where $\beta = (k_BT)^{-1}$ and T is the electronic temperature. The FCA due to oblique inter-subband transitions is proportional to electron population of the initial subband, a general result. The factor $\left(1 - e^{-\beta\hbar\omega}\right)$ accounts for the stimulated emission. Note that it is far from being negligible in the THz range because the argument of the exponential can be of the order of 1. We recover in (40) the expected feature that if the alloy scattering occurs in the barrier it will essentially be negligible. We show

in figure 9 the $\hbar\omega$ dependence of the oblique inter-subband absorption coefficient due to alloy scattering in a (Ga,In)As/Ga(As,Sb) DQW. In practice, only the scattering in the (Ga,In)As wells is important. The absorption coefficient is only a few cm^{-1} to be compared to the 10^3 cm^{-1} of the allowed (vertical in $\vec{k}$ space) inter-subband transition. Of course, near the threshold $E_3 - E_2$ the oblique in $\vec{k}$ absorption becomes large but one faces difficulties with collision broadening since the latter is not properly included in (40-41). Far from resonance, when the empirical absorption coefficient has no reason to be valid the perturbative approach provides a reliable estimate of the absorption. **Notice that the weak absorption limit in which we are working is justified by the result of the calculation of k_1/k_2 (where $k = k_1 + ik_2$ is the wavevector of the electromagnetic wave) shown in the lower panel of figure 9. One sees very clearly that this ratio exceeds 10 except in the immediate vicinity of the intersubband absorption where the perturbative estimate (that generates the divergency) becomes unreliable.**

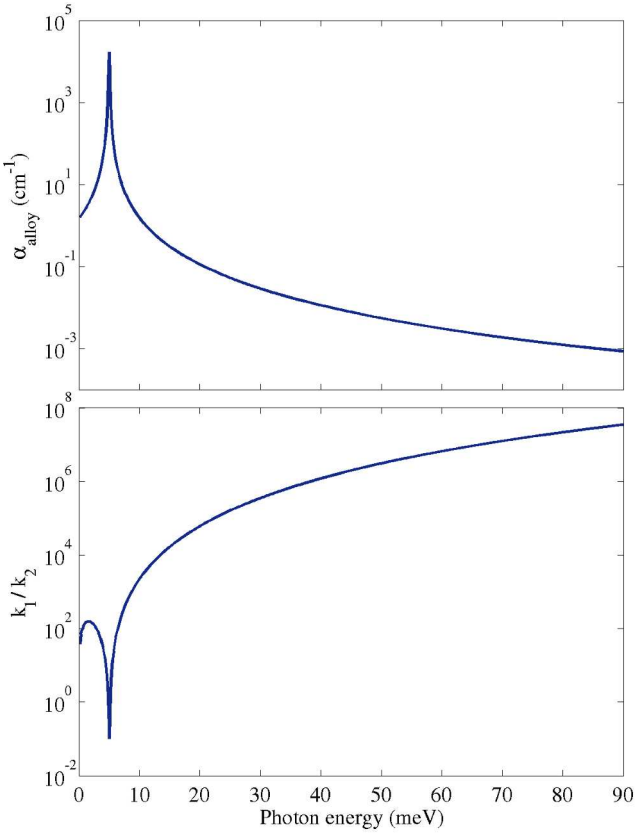

Figure 9. (higer panel)The inter-subband absorption coefficient due to oblique in $\vec{k}$ transitions assisted by alloy scattering is plotted versus the photon energy $\hbar\omega$ in a $Ga_{0.47}In_{0.53}As/GaAs_{0.48}Sb_{0.52}$ 23.2/3.1/9.8 nm DQW n_2=2.17×10^{10} cm^{-2}. T=100 K. (lower panel) The ratio k_1/k_2 versus the photon energy calculated for the same structure with the refractive index n_r=3.7.

For the Gaussian interface defects, one obtains after averaging over the positions

of the defects in the layer plane:

$$\alpha_{ij}^{def} = \frac{\pi e^2 n_2 V_b^2 \sigma^4}{\varepsilon_0 c n_r m^* L_z \hbar} \left(1 - e^{-\beta\hbar\omega}\right) \times \frac{|\langle 2|p_z|3\rangle|^2}{\hbar\omega} R_{ij}(\omega) I_{ij}^{def}(\omega) \tag{42}$$

R_{ij} is a resonant factor for intra-subband ($i = j$) and inter-subband ($i \neq j$) transitions:

$$\begin{aligned} R_{22}(\omega) &= \left(\frac{1}{\hbar\omega - E_3 + E_2} + \frac{1}{\hbar\omega + E_3 - E_2}\right)^2 \\ R_{23}(\omega) &= \left(\frac{1}{\hbar\omega - E_3 + E_2}\right)^2 \end{aligned} \tag{43}$$

and

$$\begin{aligned} I_{ij}^{def}(\omega) &= \phi_{ij}(\omega) \int_0^\infty dx e^{-x(1+C)} I_0\left[C\sqrt{x^2 + \beta x(\hbar\omega - E_j + E_i)}\right] \\ &\quad \times Y(x + \beta(\hbar\omega - E_j + E_i)) \\ \phi_{ij}(\omega) &= 2\pi F_{ij}^{def} \exp\left(-\frac{2m^*\sigma^2(\hbar\omega - E_j + E_i)}{\hbar^2}\right) \quad ; \quad C = \frac{4m^*\sigma^2}{\beta\hbar^2} \end{aligned} \tag{44}$$

where I_0 is the Bessel function of order zero with an imaginary argument and where:

$$\begin{aligned} F_{22}^{def} &= \sum_{z_0} \left(n_{att} \left|\int_{z_0 - h_{def}}^{z_0} dz \chi_3 \chi_2\right|^2 + n_{rep} \left|\int_{z_0}^{z_0 + h_{def}} dz \chi_3 \chi_2\right|^2\right) \\ F_{23}^{def} &= \sum_{z_0} \left(n_{att} \left|\int_{z_0 - h_{def}}^{z_0} dz (\chi_3^2 - \chi_2^2)\right|^2 + n_{rep} \left|\int_{z_0}^{z_0 + h_{def}} dz (\chi_3^2 - \chi_2^2)\right|^2\right) \end{aligned} \tag{45}$$

The F's account for the values of the wavefunctions associated with the states involved in the virtual coupling, close to the disordered interfaces. We see that the intra-subband F requires both the wavefunctions to be sizeable while the inter-subband F needs only one to be sizeable. That is why the absorption coefficient associated with the oblique inter-subband transitions is larger than the one associated with intra-subband transitions. Again, we find that the interface roughness intra-subband and inter-subband absorptions have no Drude-like ω^{-p} features but a resonance at the $E_3 - E_2$ transition energy. We show in figure 10 the $\hbar\omega$ dependence of the absorption coefficient for E_2-E_2 and E_2-E_3 absorption in a 23.2/3.2/9.8 nm GaAs/$Ga_{0.85}Al_{0.15}As$ DQW. In this structure the $E_2 - E_1$ lasing energy is 16.9 meV. We evidence in figure 11 the importance of the F_{ij} terms on the magnitude of the assisted absorption coefficient by plotting the L_2 dependence of α_{22}^{def} at the lasing energy $\hbar\omega = E_2 - E_1$ in a 23.2 nm/3.1nm/L_2 GaAs/$Ga_{0.85}Al_{0.15}As$ DQW.

The contributions of ionized impurities to oblique transitions are handled like those due to roughness scattering. We find for unscreened impurities located on the planes z=z_l ($z_l = 0$ corresponds to the first barrier/well interface of the DQW structure):

$$\alpha_{ij}^{imp}(\omega) = \frac{e^6 n_2 \left(1 - e^{-\beta\hbar\omega}\right)}{16\pi\varepsilon_0^3\varepsilon_r^2 c n_r m^* L_z \hbar} \times \frac{|\langle 2|p_z|3\rangle|^2}{\hbar\omega} R_{ij}(\omega) I_{ij}^{imp}(\omega)$$

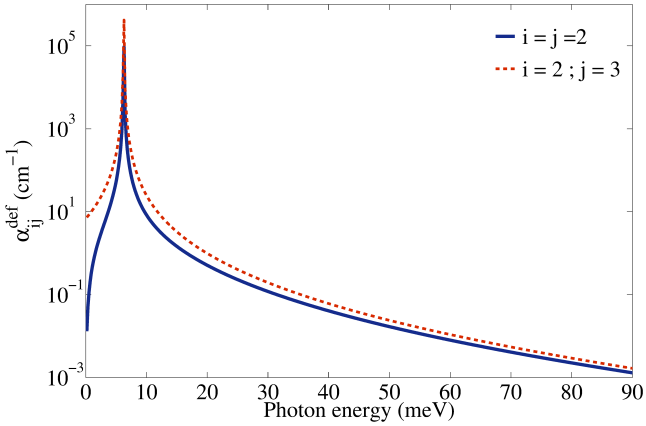

Figure 10. Photon energy $\hbar\omega$ dependence of the absorption coefficient in presence of interface defects for E_2-E_2 and E_2-E_3 oblique absorptions in a 23.2/3.1/9.8 nm GaAs/$Ga_{0.85}Al_{0.15}$As DQW. The interface roughness parameters are: σ=3.6 nm, f_r=0.3 and h_{def}=0.283 nm. The defects are placed on the two inner interfaces of the DQW. n_2=2.17×10^{10} cm^{-2}. T=100 K.

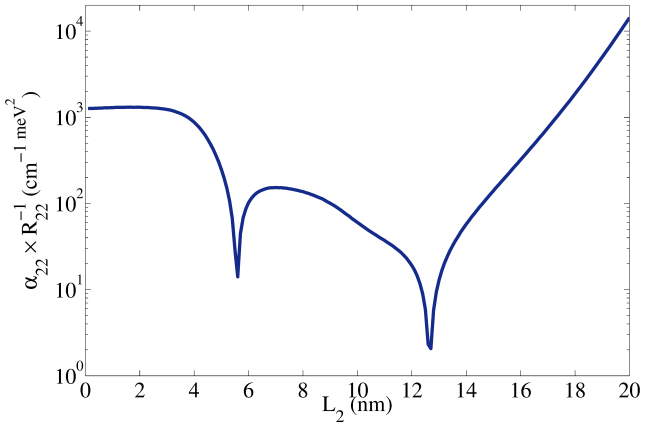

Figure 11. $\alpha_{22}^{def} \times R_{22}^{-1}(\hbar\omega = E_2 - E_1)$ versus L_2 in a 23.2 nm/3.1 nm/L_2 GaAs/$Ga_{0.85}Al_{0.15}$As DQW structure.The interface roughness parameters are: σ=3.6 nm, f_r=0.3 and h_{def}=0.283 nm. The defects are placed on the two inner interfaces of the DQW. n_2=2.17×10^{10} cm^{-2}. T=100 K.

$$I_{ij}^{imp}(\omega) = \sum_{z_l} n_{imp}^{2D}(z_l) \int_0^\infty dx e^{-x} Y\left[x + \beta(\hbar\omega - E_j + E_i)\right] \times \int_0^{2\pi} d\theta \frac{F_{ij}^{imp}(Q_{ij}(x,\theta,\omega), z_l)}{Q_{ij}^2(x,\theta,\omega)} \tag{46}$$

where the resonant factors R_{ij} have been defined previously and:

$$Q_{ij}^2(x,\theta,\omega) = \frac{2m^*}{\hbar^2\beta}\left[2x + \beta(\hbar\omega - E_j + E_i) - 2\cos\theta\sqrt{x^2 + \beta x(\hbar\omega - E_j + E_i)}\right]$$
$$F_{22}^{imp}(Q_{22}) = \int dz \chi_2(z)\chi_3(z) e^{-Q_{22}|z-z_l|}$$
$$F_{23}^{imp}(Q_{23}) = \int dz [\chi_3^2(z) - \chi_2^2(z)] e^{-Q_{23}|z-z_l|} \tag{47}$$

We show in figure 12 the importance of the impurity location on the strength of the oblique transitions in the 23.2/3.2/9.8 nm GaAs/$Ga_{0.85}Al_{0.15}As$ DQW structure. In figure 12 there is a single impurity plane and we show the magnitude of the absorption coefficient at the lasing energy versus the location z_l of the impurity plane. It is seen that one may find dopant locations that inhibit the losses due to intra-subband and inter-subband oblique transitions.

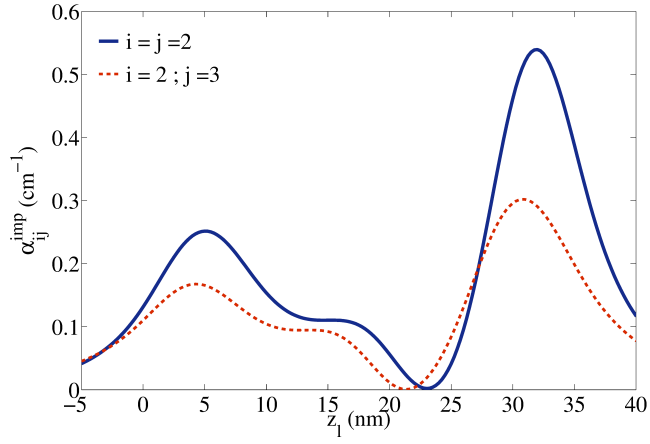

Figure 12. Absorption coefficient at the lasing $E_2 - E_1$ transition energy versus the impurity location z_l in a 23.2/3.1/9.8 nm GaAs/$Ga_{0.85}Al_{0.15}As$ DQW structure. n_2=2.17×10^{10} cm^{-2}. T=100 K.

The most efficient inelastic scattering arises from the Fröhlich coupling between electrons and LO phonons. Let us assume monochromatic bulk-like LO phonons and denote by T_L and T the lattice and the electron temperatures and by $\beta_L = (k_B T_L)^{-1}$. The absorption coefficient for LO phonon absorption is given by:

$$\alpha_{ij}^{LO\ abs}(\omega) = \frac{e^4 n_2 \omega_{LO}}{16\pi\varepsilon_0^2\varepsilon_r c n_r m^* L_z} N_{LO} \frac{|\langle 2|p_z|3\rangle|^2}{\hbar\omega} R_{ij}(\omega) S_{ij}(\omega)$$
$$S_{ij}(\omega) = \left(1 - e^{-\beta\hbar\omega} e^{(\beta_L-\beta)\hbar\omega_{LO}}\right) I_{ij,K}^{LO\ abs}(\omega) + \frac{n_2\pi\hbar^2\beta}{2m^*}$$
$$\times \left(e^{-\beta\hbar\omega} e^{(\beta_L-\beta)\hbar\omega_{LO}} - e^{-\beta\hbar(\omega+\omega_{LO})}\right) I_{ij,\Xi}^{LO\ abs}(\omega) \qquad (48)$$

where N_{LO} is the Bose occupation function for the phonons and the functions $I_{ij,Q}^{LO\ abs}(\omega)$ with $Q = K$ or Ξ are given by:

$$I_{ij,Q}^{LO\ abs}(\omega) = \int_0^\infty dx e^{-x} Y\left(x + \beta(\hbar\omega + \hbar\omega_{LO} - E_j + E_i)\right)$$
$$\times \int_0^{2\pi} d\theta \frac{F_{ij}^{LO}(Q_{ij}(x,\theta,\omega))}{Q_{ij}(x,\theta,\omega)}$$
$$F_{22}^{LO} = \int\int dz\ dz' \chi_3(z)\chi_3(z')\chi_2(z)\chi_2(z') e^{-Q_{22}|z-z'|} \qquad (49)$$
$$F_{23}^{LO} = \int\int dz\ dz' [\chi_3^2(z)\chi_3^2(z') + \chi_2^2(z)\chi_2^2(z') - 2\chi_3^2(z)\chi_2^2(z')] e^{-Q_{23}|z-z'|}$$

where $Q_{ij} = K_{ij}$ or Ξ_{ij}:

$$K_{ij}^2(x,\theta,\omega) = \frac{2m^*}{\hbar^2\beta}$$

$$\times \left[2x + \beta(\hbar\omega + \hbar\omega_{LO} - E_j + E_i) - 2\cos\theta\sqrt{x^2 + \beta x(\hbar\omega + \hbar\omega_{LO} - E_j + E_i)}\right]$$

$$\Xi_{ij}^2(x,\theta,\omega) = \frac{2m^*}{\hbar^2\beta} \tag{50}$$

$$\times \left[x + \beta(\hbar\omega + \hbar\omega_{LO} - E_j + E_i) - \cos\theta\sqrt{x^2 + 2\beta x(\hbar\omega + \hbar\omega_{LO} - E_j + E_i)}\right]$$

Similar expressions are found for the oblique transitions assisted by LO phonon emission [27]. The spatial localizations of the initial and final states play a large part in the phonon assisted oblique transitions as evidenced by the F_{ij} functions. We show in figure 13 the absorption coefficient normalized by the resonant factor R_{ij} associated with the LO phonon assisted intra-subband transition in the 23.2 nm/3.2 nm/L_2 GaAs/$Ga_{0.85}Al_{0.15}As$ DQW structure at the lasing frequency when T=T_L=100 K and 300 K. There is an enhancement of the absorption for structures where χ_2 and χ_3 delocalise due to level anticrossing $L_2 \approx 9$ nm.

Finally, it is interesting to compare the contributions of the various processes to oblique transitions. We show in figure 14 the calculated inter-subband absorption in a triple well structure based on ternary materials (Ga,In)As/Ga(As,Sb) where two monolayers interface defects have been assumed with a fractional coverage of f_r=0.3. The LO phonon energy was chosen equal to 34 meV and the impurity concentration was 1.5×10^{10} cm^{-2}. T_L=T=100 K and 300 K. The plots of figure 14 display a divergence at the subband energy difference ($\hbar\omega \approx 55$ meV). For the LO phonon absorption mechanism, we also note a second peak at $\hbar\omega \approx 21$ meV which corresponds to a coulombic divergence that occurs when $\hbar\omega = E_2 - E_1 - \hbar\omega_{LO}$.

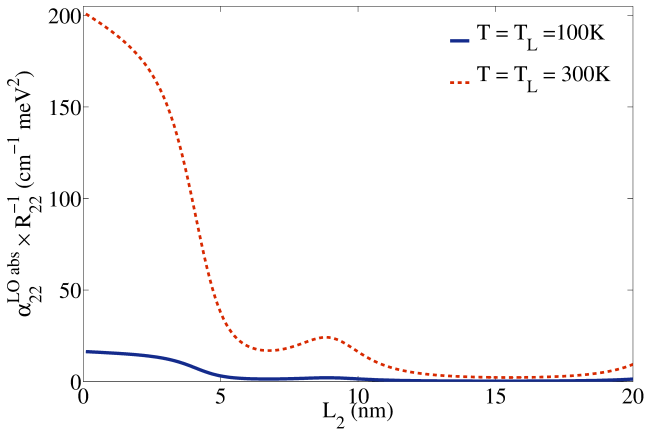

Figure 13. $\alpha_{22}^{LOabs} \times R_{22}^{-1}$ associated with the LO phonon assisted intra-subband transition in a 23.2 nm/3.1 nm/L_2 GaAs/$Ga_{0.85}Al_{0.15}As$ DQW structure at the lasing energy $E_2 - E_1$ when T=T_L=100 K and 300 K. $\hbar\omega_{LO}$=36 meV. n_2=2.17×10^{10} cm^{-2}.

The most striking feature displayed in figure 14 is the relative smallness of the absorption due to oblique transitions. While tens or hundreds of cm^{-1} come from a blind application of the 3D Drude model, actual calculations performed for realistic structures point out that FCA ≤ 20 cm^{-1} out of resonance in most QCL structures. Hence, the laser

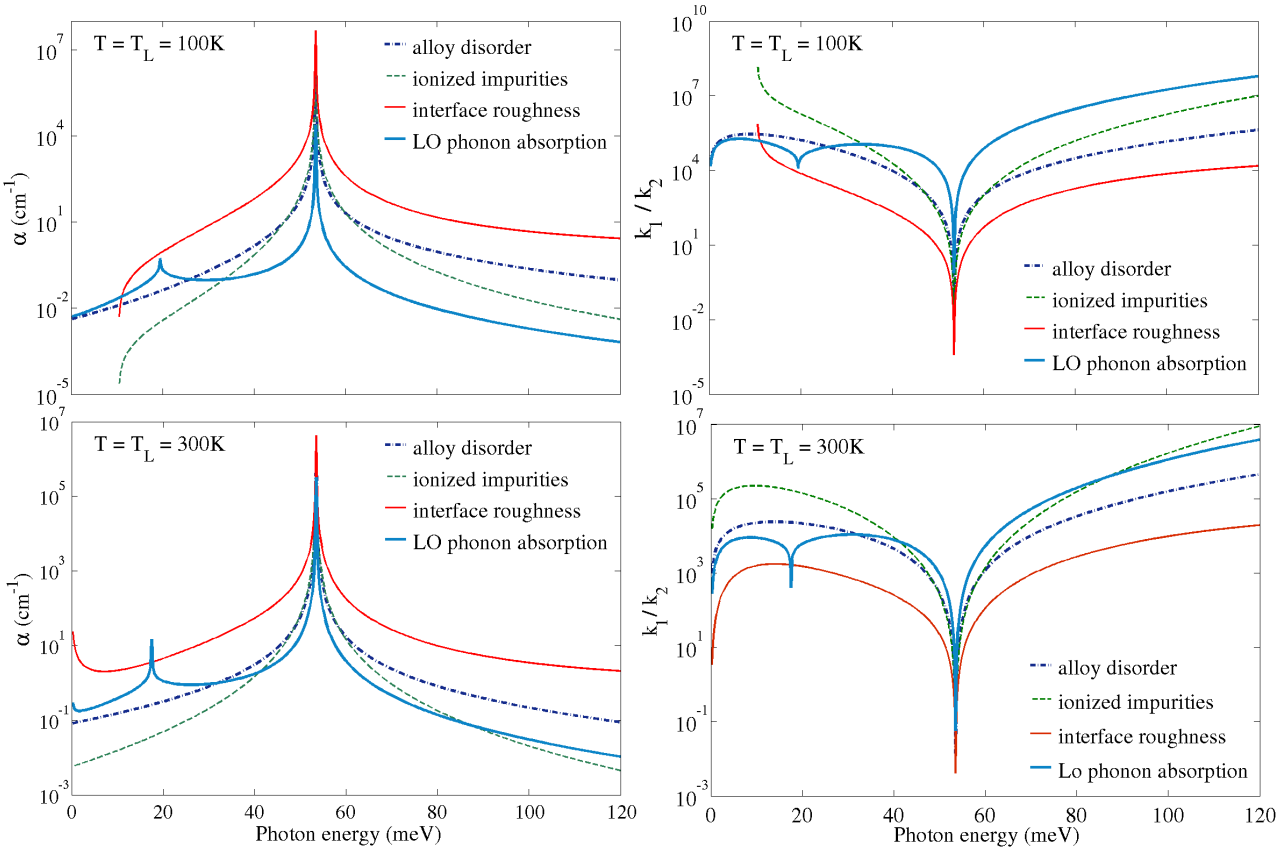

Figure 14. (right panel) Calculated E_4-E_5 inter-subband absorption in a 12.5/0.9/11.7/2.6/21.0 biased triple well structure based on ternary materials (Ga,In)As/Ga(As,Sb). The lasing energy is $E_2 - E_1$=15.3 meV. F=12 kV/cm. (left panel) The ratio k_1/k_2 versus the photon energy calculated for the same structure with the refractive index n_r=3.7.

re-absorption by the free carriers of the QCL structures is comparable to the losses in the cladding waveguide. The small FCA is the result of the very low carrier concentrations in these structures (a few 10^{10} cm^{-2}) and of the excellent control of the layers and their interfaces. At $T_L < 100$ K, the dominant interaction processes causing FCA are elastic scatterers while above 200 K the electron-LO phonon dominates at the lasing energy. In GaAs based materials, interface roughness appears to be dominated by intentionally placed dopants while in heterostructures with no common anion, like InAs/AlSb, it appears that the interface roughness is a more likely cause of FCA. The alloy scattering, essentially inexistent in a GaAs-based heterostructures is a very important process in ternary-based QCL's. It appears clear that there is still some room for improving QCL structures since neither the materials, nor the designs are at their best yet [40].

3.5. Green's function approach to oblique optical transitions.

The Green's function approach allows for a self-consistent treatment of level broadening effects and is thus particularly appropriate for the study of optical transitions far from

resonance. The central idea is to focus on the lesser Green's function (for details, see Ref. [10])

$$G^<_{\alpha\beta}(\vec{k};t_1,t_2) = \mathrm{i}\langle \hat{a}^\dagger_{\beta\vec{k}}(t_2)\hat{a}_{\alpha\vec{k}}(t_1)\rangle\,. \tag{51}$$

This is a generalisation of the standard density matrix towards two different time arguments in the annihilation ($\hat{a}_{\alpha\vec{k}}(t)$) and creation ($\hat{a}^\dagger_{\alpha\vec{k}}(t)$) operator for the state with wavevector $\vec{k}$ in subband α within the Heisenberg picture. In a stationary state (here indicated by a tilde), the Green's function depends only on the time difference $t_1 - t_2$ and can be written as

$$\tilde{G}^<_{\alpha\beta}(\vec{k};t_1,t_2) = \int \frac{\mathrm{d}E}{2\pi}\tilde{G}^<_{\alpha\beta}(\vec{k},E)\mathrm{e}^{-\mathrm{i}E(t_1-t_2)/\hbar}\,. \tag{52}$$

This energy dependence (i.e., the Fourier parameter E) displays the distribution of occupation over energy in a broadened state. In thermal equilibrium, the diagonal elements dominate and are given by

$$\tilde{G}^<_{\alpha\alpha}(\vec{k},E) = if_f(E)A^{\mathrm{ret}}_\alpha(\vec{k},E) \tag{53}$$

where $0 \le f_f(E) \le 1$ is the Fermi function and the spectral function describing the broadening of the subband state $\alpha,\vec{k}$ reads

$$A_\alpha(\vec{k},E)) = \pm 2\Im\left\{\tilde{G}^{\mathrm{adv/ret}}_{\alpha\alpha}(\vec{k},E))\right\} = \frac{\Gamma_\alpha(\vec{k},E)}{[E-\epsilon_{\alpha\vec{k}}-R_\alpha(\vec{k},E)]^2-\Gamma^2_\alpha(\vec{k},E)/4} \tag{54}$$

where $\Gamma_\alpha(\vec{k},E) = \pm 2\Im\{\tilde{\Sigma}^{\mathrm{adv/ret}}_{\alpha\alpha}(\vec{k},E))\}$ and $R_\alpha(\vec{k},E) = \Re\{\tilde{\Sigma}^{\mathrm{adv/ret}}_{\alpha\alpha}(\vec{k},E))$. These self-energies Σ take into account scattering processes, where $\Gamma_\alpha(\vec{k},E)/\hbar$ corresponds to the total scattering rate and provides the full width at half maximum of the spectral function. We see, that this energy dependence naturally represents broadened states. However, one has to pay the price that the energy E appears as an independent variable in addition to the state indices α and k, which requires strong effort on numerical schemes. The basis of our numerical calculations is outlined in Ref. [41] where the full non-diagonal structure of Green's functions and self-energies is taken into account, while for the analytical considerations in this section, we focus on the diagonal spectral functions A_α for the equilibrium state.

A perturbation potential $eF_{\mathrm{ac}}\hat{z}e^{-i\omega t}$ ($e > 0$ is the elementary charge) corresponds to the electromagnetic field (here in Lorenz gauge [42] and long-wave approximation), for electromagnetic fields with a polarisation of the electrical field perpendicular to the layers. In linear response this provides a lesser Green's function

$$G^<_{\alpha\beta}(\vec{k},t_1,t_2) = \tilde{G}^<_{\alpha\beta}(\vec{k};t_1,t_2) + \int \frac{\mathrm{d}E}{2\pi}\delta G^<_{\alpha\beta}(\vec{k},\omega,E)\mathrm{e}^{-\mathrm{i}E(t_1-t_2)/\hbar}\mathrm{e}^{-\mathrm{i}\omega t_1} \tag{55}$$

By evaluating the dynamical conductivity, one obtains the absorption coefficient [42]

$$\alpha(\omega) = -\frac{2e}{c\hbar\epsilon_0 n_r F_{\mathrm{ac}} A L_z}\Re\left\{\sum_{\alpha\beta,\vec{k}}\int\frac{\mathrm{d}E}{2\pi}W_{\beta\alpha}\delta G^<_{\alpha\beta}(\vec{k},\omega,E)\right\} \tag{56}$$

where‖

$$W_{\beta\alpha} = -\hbar^2 \int \mathrm{d}z\, \varphi^*_\beta(z) \frac{1}{m^*(z)} \frac{\partial}{\partial z} \varphi_\alpha(z) = (E_\beta - E_\alpha) z_{\beta\alpha}$$

with the subband energies E_α and E_β. In linear response with respect to the ac field we find [42]:

$$\begin{aligned}
\delta\boldsymbol{G}^<(\vec{k},\omega,E) = {} & \tilde{\boldsymbol{G}}^{\mathrm{ret}}(\vec{k},E+\hbar\omega)\delta\boldsymbol{U}(\omega)\tilde{\boldsymbol{G}}^<(\vec{k},E) \\
& + \tilde{\boldsymbol{G}}^<(\vec{k},E+\hbar\omega)\delta\boldsymbol{U}(\omega)\tilde{\boldsymbol{G}}^{\mathrm{adv}}(\vec{k},E) \\
& + \tilde{\boldsymbol{G}}^{\mathrm{ret}}(\vec{k},E+\hbar\omega)\delta\boldsymbol{\Sigma}^{\mathrm{ret}}(\vec{k},\omega,E)\tilde{\boldsymbol{G}}^<(\vec{k},E) \\
& + \tilde{\boldsymbol{G}}^{\mathrm{ret}}(\vec{k},E+\hbar\omega)\delta\boldsymbol{\Sigma}^<(\vec{k},\omega,E)\tilde{\boldsymbol{G}}^{\mathrm{adv}}(\vec{k},E) \\
& + \tilde{\boldsymbol{G}}^<(\vec{k},E+\hbar\omega)\delta\boldsymbol{\Sigma}^{\mathrm{adv}}(\vec{k},\omega,E)\tilde{\boldsymbol{G}}^{\mathrm{adv}}(\vec{k},E)\,, \qquad (57)
\end{aligned}$$

where the capital bold-face symbols are matrices in the subband indices α, β and $\delta\mathbf{U}(\omega) = eF_{\mathrm{ac}} z_{\alpha\beta}$ in $\vec{E}\cdot\hat{d}$ coupling. Neglecting the changes of the self-energies $\delta\boldsymbol{\Sigma}$, assuming diagonal stationary Green's functions $\tilde{G}$, and considering only two subbands $\alpha = 1, 2$, we thus obtain

$$\begin{aligned}
\alpha(\omega) = {} & \frac{e^2|z_{21}|^2(E_2-E_1)}{c\hbar\epsilon_0 n_r A L_z} \sum_{\vec{k}} \int \frac{\mathrm{d}E}{2\pi} [f_F(E) - f_F(E+\hbar\omega)] \\
& \times \left[A_2(\vec{k},E+\hbar\omega) A_1(\vec{k},E) - A_1(\vec{k},E+\hbar\omega) A_2(\vec{k},E) \right] \qquad (58)
\end{aligned}$$

This equation is visualised in Fig. 15, displaying the essential origin of the linewidth and -shape for intersubband transitions. For $E_2 > E_1$ the term $\tilde{A}_1(\vec{k},E+\hbar\omega)\tilde{A}_2(\vec{k},E)$ is the counter-rotating term. If one uses $\vec{A}\cdot\hat{p}$ coupling (corresponding to Coulomb gauge [42]), one obtains an additional factor $(E_2-E_1)/\hbar\omega$ and a sign change in the counter-rotating term. Numerically, both approaches provide very similar results, if a sufficiently large basis is applied [41, 42]. It appears that the $\vec{E}\cdot\hat{d}$ coupling via $\delta\mathbf{U}(\omega) = eF_{\mathrm{ac}} z_{\alpha\beta}$ is more stable because there is no diverging factor $1/\omega$ in the beginning.

Assuming constant values $\Gamma_\alpha(\vec{k},E) \approx \Gamma_\alpha$ as well as constant occupation functions $f_F(E) \approx f_F(\epsilon_{\alpha\vec{k}})$ in the range of the respective spectral functions, and omitting the counter-rotating term (which is the rotating wave approximation) we find

$$\alpha(\omega) \approx \frac{e^2|z_{21}|^2(E_2-E_1)}{c\hbar\epsilon_0 n_r A L_z} \sum_{\vec{k}} \frac{\Gamma_2+\Gamma_1}{(E_1+\hbar\omega-E_2)^2 + (\Gamma_2+\Gamma_1)^2/4} [f_F(\epsilon_{1\vec{k}}) - f_F(\epsilon_{2\vec{k}})] \qquad (59)$$

which is essentially Eq. (32), if one replaces $E_2 - E_1$ by $\hbar\omega$ (actually this form can be obtained if one calculates the absorption via the susceptibility instead the conductivity as done here). However, the full Green's function approach contains several corrections to this simplified result:

- The energy dependence of the Fermi functions, provide a slight blue shift of the spectrum, as one can immediately see from Fig. 15. This is directly related to the dispersive gain addressed in [43], see also [44].

‖ This definition of W equals [42]. It corresponds to $L_z W_{\mathrm{prev}}$ for the expression W_{prev} used in [41], where the average is taken over the length L_z covering all states.

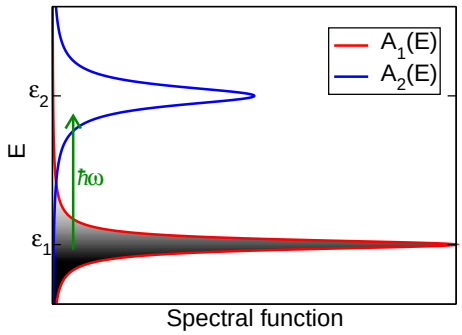

Figure 15. Sketch of absorption as evaluated by Eq. (58) for a fixed $\vec{k}$. The grey scale provides the occupation function $f_F(E)$. The total absorption is the sum of all upward arrows weighted with the product of spectral functions and the difference in occupations taken at start and end point.

- The self-energies $\tilde{\Sigma}_{\alpha\alpha}(\vec{k}, E)$ are not constant. For elastic scattering with scattering matrix elements $V_{\alpha\beta}(\vec{q})$ we find within the Born approximation (here not self-consistent)

$$\Gamma_\alpha(\vec{k}, E) = 2\pi \sum_{\beta\vec{k}'} |V_{\beta,\alpha}(\vec{k} - \vec{k}')|^2 \delta(E - \epsilon_{\beta\vec{k}'})$$

  Thus the term with $\beta = \alpha$ vanishes for $E < \epsilon_{\alpha\vec{0}}$ and the spectral functions become very asymmetric for small $\vec{k}$. (Higher-order corrections starting with the self-consistent Born approximation provide finite values also for a small range of energies below $\epsilon_{\alpha\vec{0}}$.) For the oblique transitions with $\hbar\omega \ll E_2 - E_1$ we find

$$\alpha(\omega) = \frac{e^2|z_{21}|^2(E_2 - E_1)}{c\hbar\epsilon_0 n_r A L_z} \sum_{\vec{k}\vec{k}'} \left[f_F(\epsilon_{1\vec{k}}) - f_F(\epsilon_{1\vec{k}'})\right] \frac{2\pi|V_{1,2}(\vec{k} - \vec{k}')|^2 \delta(\epsilon_{1\vec{k}'} + \hbar\omega - \epsilon_{1\vec{k}'})}{(E_1 + \hbar\omega - E_2)^2}$$

  These correspond to the oblique intersubband transitions addressed in Sec. 3.4.

- The width of the spectrum is reduced due to the terms $\delta\boldsymbol{\Sigma}$ Eq. (57), which had been neglected in obtaining Eq. (58). As shown in [39], for special situations one finds a width proportional to the scattering matrix elements $|V_{11} - V_{22}|^2$ as already noticed by [45].

3.6. Link between FCA and inter-subband absorption tail. Comparison between different approaches

The intersubband absorption lineshape in an imperfect heterostructure results from two combined effects. On the one hand, the static or dynamic disorder blurs the eigenenergies of the system and results in a lineshape that is no longer described by a delta function. Simultaneously, the static and dynamic disorder breaks the translation invariance in the layer plane, which results in the possibility to observe oblique transitions. Let us consider the absorption of a photon with energy $\hbar\omega < E_2 - E_1$. The question we address in this paragraph is to know to which extent the absorption process results from the blurring of the energy conservation or from tthe breakdown of the optical selection rules.

We shall see that depending on the magnitude of $\hbar\omega$ versus $E_2 - E_1$ one or the other mechanism prevails: close to $E_2 - E_1$, the absorption mainly arises from the blurring of the eigenenergies while, far detuned from $E_2 - E_1$, it is the existence of oblique transitions that triggers the photon absorption. A complete numerical calculation will be very useful in ascertaining the respective parts played by the two mechanisms.

A convenient way to envision FCA for the intra-subband transition is to consider it as the low energy tail of an absorption spectrum (see figure 16). Hence, we would find from (34) an intra-subband absorption at $\hbar\omega$ equal to:

$$\alpha_{intra}(\hbar\omega) \equiv \alpha_{inter}(\hbar\omega) \approx \alpha_{inter}(E_2 - E_1)\frac{\hbar\omega\Gamma^2}{(E_2 - E_1)^2} \tag{60}$$

where we have assumed $E_2 - E_1 \gg \hbar\omega$. With the same parameters as used in (34) we find for a photon energy $\hbar\omega$=10 meV an absorption coefficient of 0.16 cm^{-1}. Here we neglected the energy dependence of occupations in the subbands for simplicity, which could be taken into account by a detailed density matrix theory [43] or Green's function technique as discussed above. As expected, we find a tail that is the more intense when the inter-subband line is the broader. The order of magnitude of the absorption is too large compared to microscopic calculations and this originates from the inability of (34) to account for the doubly forbidden nature of the intra-subband absorption. Actually, microscopic variants of (34) were obtained by Unuma *et al* [38], following Ando [3]. In Unuma *et al* 's model the parameter Γ acquires a status of material related quantity that can be calculated if one knows the elastic scatterers, phonons etc..(see eqs. (25) in [38]).

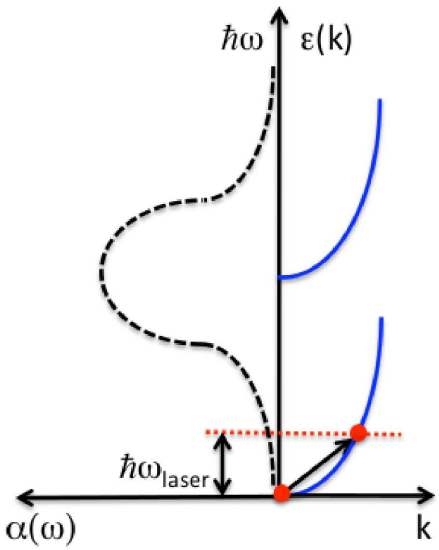

Figure 16. Right panel: dispersion relation $\varepsilon(k)$ versus k and intra-subband absorption process. Left panel: absorption coefficient $\alpha(\omega)$ (dashed line) versus photon energy corresponding to an inter-subband transition.

As explained in section 3.5, the Keldysh Green's function formalism can be implemented to compute the optical conductivity and the absorption coefficient. It

is interesting to compare the outputs of the different models on a specific case [46]. We consider the case of a 9/2/3 nm GaAs/$Ga_{0.75}Al_{0.25}As$ DQW with Gaussian interface defects placed on the two inner interfaces. These defects are characterized by the parameters σ=3.6 nm and f_r=0.3. We show in figure 17 the absorption coefficient of the DQW based on a numerical exact solution of the Hamiltonian H_{eff} (4) in presence of interface defects [46](blue solid line). In all the plots shown in figure 17 the delta function of energy conservation in the expression for the absorption coefficient $\alpha(\omega)$ has been replaced by a gaussian with full width at half maximum of 1.8 meV. It is compared to the perturbative approach outlined in sections 3.3 and 3.4 (green dashed line). The red solid line (dashed-dotted blue line) corresponds to a numerical calculation of the initial and final states that includes only the intra-subband (inter-subband) matrix elements of the interface defect potential. We see very clearly that the intra-subband scattering controls the center of the absorption spectrum and the high energy tail, but completely fails to account for the low energy absorption tail. Symmetrically, the inter-subband scattering plays a negligible part in the build up of the center and the high energy tail of the absorption spectrum but is overwhelming in the low energy tail. This result agrees with the formulation developped for the perturbative model (section 3.4): eqs.(37)-(39) show that intra-subband oblique optical transitions occour thanks to inter-subband scattering, while inter-subband oblique optical transitions are assisted by intra-subband scattering. Note that this clear dichotomy between the parts played by the intra-subband and inter-subband matrix elements is likely to become invalidated when going towards the THz range because $E_2 - E_1$ will be of the same order of magnitude as the typical interface defect inter-subband matrix elements $\langle n\vec{k}|\delta V_{def}|\vec{k'}n'\rangle$, while the case in figure 17 corresponds to $E_2 - E_1 \gg \langle n\vec{k}|\delta V_{def}|\vec{k'}n'\rangle$.

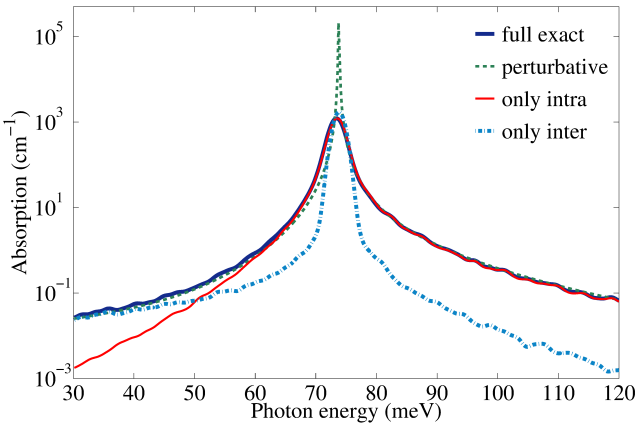

Figure 17. Absorption spectrum for the E_1-E_2 transition calculated by: fully numerical diagonalization (blue solid line); taking into account either only the intra-subband matrix elements $\langle n\vec{k}|\delta V_{def}|\vec{k'}n\rangle$ (red solid line) or only the inter-subband ones $\langle n\vec{k}|\delta V_{def}|\vec{k'}n'\rangle$ (blue dashed-dotted line); and by expanding the electron wavefunction to the first order in both $\langle n\vec{k}|\delta V_{def}|\vec{k'}n\rangle$ and $\langle n\vec{k}|\delta V_{def}|\vec{k'}n'\rangle$ (green dashed line). $T = 100$ K. Reprinted with permission from [46]. Copyright 2012, American Institute of Physics.

While it is interesting to understand which physical effects controls the center and the wings of the absorption line, it is also important to ascertain the validity of approximate but useful derivations against exact numerical calculations. We show in figure 18 the absorption line computed either numerically by exact diagonalization (blue solid line), by using the Keldysh formalism (CRF_1) or by the Unuma model (CRF_2) [38]. We see that CRF_1 (red solid line) gives a good description of the low ω behavior. On the other hand CRF_1 fails at large energy because of the approximation in the numerics of all matrix elements by those of delta scatterers. This approximation overestimates the scattering at large k compared to the regular Gaussian interface defects. In CRF_2, we use Unuma's approach for the inter-subband absorption coefficient by converting its real part of the frequency dependent conductivity into an absorption coefficient using (2) and (3). It is clear that CRF_2 poorly describes the FCA far from resonance. The difference between CRF_1 and CRF_2 probably arises from the fact that CRF_2 neglects the off diagonal components of the Green's function, i.e. the wavefunction admixture due to the interface disorder that we have seen to be important for the absorption tails. Close from the maximum of the inter-subband absorption, where the broadening is dominated by intra-subband scattering, both correlation function models work well since the wavefunction admixture is a negligible effect compared to the blurring of the eigenstates.

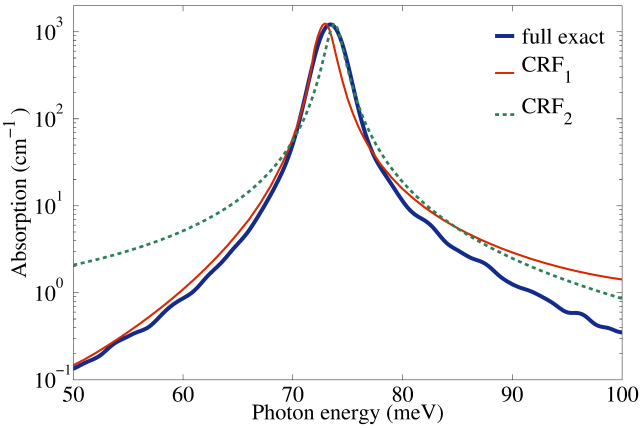

Figure 18. Absorption spectrum for the E_1-E_2 transition calculated by three different models: exact diagonalization (blue solid line), Keldysh Green's function formalism, CRF_1 (red solid line), Unumas model, CRF_2 (green dashed line). $T = 100$ K.Reprinted with permission from [46]. Copyright 2012, American Institute of Physics.

3.7. From intersubband transitions to bulk free carrier absorption

The transition towards the bulk free-carrier absorption can be understood within a two-step process as outlined in [11]. If one considers multiple quantum well structures, there is a multitude of low lying states, which provide a rather broad spectrum at low frequencies. In the limit of an infinite superlattice this provides the standard Drude

form with the superlattice conductivity. Reducing the barrier width, this conductivity increases and eventually approaches the bulk value. This clearly shows, that the intersubband transitions include the entire absorption provided the obliques transitions are properly taken into account.

3.8. Existence of quasi-selection rules in imperfect heterolayers

It is known since some time from Green's function, density matrix or Boltzmann-like approaches that the relevant quantity to ascertain the broadening of inter-subband transitions involves the difference between the matrix elements of disorder between the subband states that are connected by the photon [45]. Let us start with a simple case and consider the situation where the level broadening of each of the involved subbands is controlled by interface defects and where the carrier concentration is sufficiently small to assume a Boltzmann equilibrium of the electrons. In addition, we assume that a very strong magnetic field is applied parallel to the growth axis (magnetic quantum limit). This situation is easily reached in actual QCL's and one can even find THz QCL's where the magnetic quantization $\hbar\omega_c$ becomes larger than the subband spacing [47–50]. We denote by $|i,p,\alpha\rangle$ the exact eigenstates (with energies $E_i+(p+1/2)\hbar\omega_c+\varepsilon_\alpha$) of the intra-subband Hamiltonians H_i in the presence of magnetic field and interface defects:

$$\begin{aligned} &H_i = P_i H P_i \quad ; \quad P_i = \sum_\alpha |i,p,\alpha\rangle\langle i,p,\alpha| \\ &\langle\vec{r}|i,p,\alpha\rangle = \chi_i(z)\sum_{k_y} c_i^\alpha(k_y)\frac{e^{ik_y y}}{\sqrt{L_y}}\varphi_p(x+\lambda^2 k_y) \end{aligned} \tag{61}$$

where H is the complete effective Hamiltonian excluding the coupling to the light but including the interface roughness and the magnetic field. φ_p is the Hermite function given at (11) and p is the Landau level index. In principle, the summation in (61) should also comprise a summation on the Landau level index p. In the magnetic quantum limit however there is very little Landau level mixing due to interface roughness and we shall neglect it. Along the same line, the idea that the inter-subband scattering is weak allows us to write the absorption coefficient from the states of the perturbed E_1 subband of a given Landau level p to the states of the perturbed E_2 subband of the same Landau level p as [51]:

$$\begin{aligned} \alpha_{1\to2}(\omega) \propto &|\langle 1|p_z|2\rangle|^2\left(1-e^{-\beta\hbar\omega}\right) \\ &\times\sum_{\nu,\mu}|\langle 0\nu|0\mu\rangle|^2 e^{-\beta\varepsilon_{1\nu}}\delta(E_2+\varepsilon_\mu-E_1-\varepsilon_\nu-\hbar\omega) \end{aligned} \tag{62}$$

where we have neglected the subband mixing by the interface roughness. In (62) only p=0 is populated in the magnetic quantum limit, Boltzmann statistics are used and the eigenenergies are written:

$$E_1+\frac{1}{2}\hbar\omega_c+\varepsilon_\nu \quad ; \quad E_2+\frac{1}{2}\hbar\omega_c+\varepsilon_\mu \tag{63}$$

A priori, it seems that any oblique transition $k_y \to k'_y$ between the unperturbed states is possible due to disorder. If there are N allowed k_y values, we expect there will be

N^2 possible transitions. However, we shall show that there are only N allowed optical transitions in spite of the disorder. In effect, for one interface we get using (22):

$$H_1|1,0,\nu\rangle = \sum_{k_y} c_1^{\nu}(k_y)\left(E_1 + \frac{1}{2}\hbar\omega_c + \delta V_{def}\right)|1,0,k_y\rangle$$
$$= \left(E_1 + \frac{1}{2}\hbar\omega_c + \varepsilon_\nu\right)\sum_{k_y} c_1^{\nu}(k_y)|1,0,k_y\rangle \tag{64}$$

and a similar expression for $|2,0,\mu\rangle$. (64) leads to:

$$\sum_{q_y} c_1^{\nu}\left(k_y+q_y\right)\langle 1,0,k_y|\delta V_{def}|1,0,k_y+q_y\rangle = \varepsilon_\nu c_1^{\nu}(k_y) \tag{65}$$

Evaluating the matrix elements of the interface defect potential given in (22) we obtain:

$$\langle 1,0,k_y|\delta V_{def}|1,0,k_y+q_y\rangle = V_b\frac{\sigma\sqrt{2\pi}}{L_y\sqrt{(1+r)}}\sum_{x_j,y_j}\langle 1|g(z)|1\rangle e^{iq_y y_j} \tag{66}$$
$$\times\exp\left[-\frac{\lambda^2 q_y^2}{4}\left(\frac{1}{r}+\frac{1+2r}{1+r}\right)\right]\exp\left[-\frac{(x_j+\lambda^2 k_y)^2}{2\sigma^2(1+r)}\right]\exp\left[-\frac{q_y(x_j+\lambda^2 k_y)r}{(1+r)}\right]$$

where $r = \frac{\lambda^2}{2\sigma^2}$. This expression is interesting because it shows that the separability in $\vec{\rho}$ and z of the interface roughness potential allows to re-expressing the Schrödinger equation in a dimensionless form. In fact, the coefficients $\langle 1|g(z)|1\rangle$ for attractive or repulsive defects are quite similar because the defect depth is usually much smaller than the scale of variation of the envelope function near the interface:

$$\langle 1|g(z)|1\rangle_{att} = \int_{z_0-h_{def}}^{z_0}\chi_n^2(z)dz \approx \int_{z_0}^{z_0+h_{def}}\chi_n^2(z)dz$$
$$= \langle 1|g(z)|1\rangle_{rep} \approx h_{def}\chi_n^2(z_0) \tag{67}$$

Thus, the Schrödinger equation in k_y space can be cast in the dimensionless form:

$$\sum_{q_y} c_1^{\nu}(k_y+q_y)\nu(k_y,q_y) = \eta_{1\nu}c_1^{\nu}(k_y)$$
$$\eta_{1\nu} = \frac{\varepsilon_\nu}{V_b\langle 1|g(z)|1\rangle} \quad ; \quad \nu(k_y,q_y) = \frac{\langle 1,0,k_y|\delta V_{def}|1,0,k_y+q_y\rangle}{V_b\langle 1|g(z)|1\rangle} \tag{68}$$

The dimensionless Schrödinger equation actually does not depend on the subband index. It would be the same for the motion in the p=0 Landau level of the E_2 subband. Therefore, if only one interface controls the broadening we find that the eigenstates are subband independent. This immediately implies that the quantum numbers in the two broadened Landau levels should be identical: μ=ν in (62) because the optical matrix element only affects the z dependent wavefunctions. Hence, we are lead to the conclusion that there exists an exact selection rule for the optical transitions, exactly like in ideal material. In our case, however, it does not result from the translation invariance along the y axis but by the fact that the disorder affects the initial and final states in the same manner. Also, in contrast with the selection rule in ideal materials that leads to a delta function for the absorption coefficient, the selection rule in heterostructures with interface roughness does not imply an infinitely narrow

absorption peak. For a given quantum number ν, because the scaling factors in (68) are subband dependent, the eigenenergies in the initial and final subbands are different despite identical wavefunctions for the in-plane motion. Hence in (62) the argument of the delta function depends on the initial quantum numbers, which explains why the absorption line has a finite width. We illustrate this point in figure 19 which shows the absorption coefficient versus the photon energy in a 6/0.283/6nm GaAs/$Ga_{0.55}Al_{0.45}As$ DQW (m^*=0.07m_0 in the wells and 0.094m_0 in the barriers, V_b=0.393 eV) at different magnetic fields and T=5 K or T=20 K. The eigenstates are obtained numerically by diagonalization in a 200 nm × 200 nm grid using periodic plane wave basis. The ideal DQW has a B and T independent inter-subband transition energy at E_2-E_1=59.95 meV (left vertical bar in figure 19). The interface defects have a characteristic in-plane extension of 10.8 nm, f_r=0.15 and a width of one monolayer (0.283 nm). The effect of the interface defects located on the outer interfaces is negligible and the width of the $E_1 \rightarrow E_2$ inter-subband transition is dominated by the interface roughness on the central barrier. Each Landau level is broadened because of the interface roughness but the ground subband is much more broadened than the excited one on account of the $\chi_1(z)$ ($\chi_2(z)$) maximum (minimum) probability to find the electron at the center of the DQW (see inset of figure 19a). At low temperature and strong field, the electrons mainly occupy the lowest possible states of the initial Landau level. The selection rule forces their counterpart in the excited states to have the same quantum number. Thus, the optical transition blue shifts at fixed B by lowering T or at fixed T by increasing B. Note that with increasing B the absorption line is blue shifted towards the inter-subband transition energy (70. 2 meV) (right vertical line in figure 19)) of a SQW of width 12.283 nm which is the total extension of the DQW studied here. This means that electrons strongly localized by B on the defects of the barrier feel the z-confinement as if they were in a SQW of size $2L$+0.283 nm instead of a DQW of size L/0.283 nm/L.

The question remains to ascertain whether this selection rule survives the removal of the separability of the scattering potential and that of a small phase space associated with the quantizing magnetic field. We have found no evidence that there exists a strict selection rule for inter-subband transitions in general. However, in most structures, there exist quasi-selection rules showing that the disorder effects may to a large extent cancel in the optical spectra while they are very significant in either the initial or the final subband states.

Now we consider a 9/2/3nm GaAs/$Ga_{0.75}Al_{0.25}As$ DQW, where the second subband has a stronger overlap with the interfaces compared to the first one and focus on the case without magnetic field. We assume Gaussian interface defects with characteristic in-plane extension of 3.6 nm and a fractional coverage f_r=0.3. These defects are placed on the two inner interfaces of the structure. The Schrödinger equation including inter-subband coupling is solved numerically as described above. Figure 20 shows the in-plane probability distribution for two states with energies, respectively equal to E_1+3 meV and E_2+3 meV. The extra energies +3 meV are larger (respectively, smaller) than the typical effective in-plane potential depths in the E_1 and E_2 subbands (0.4 meV

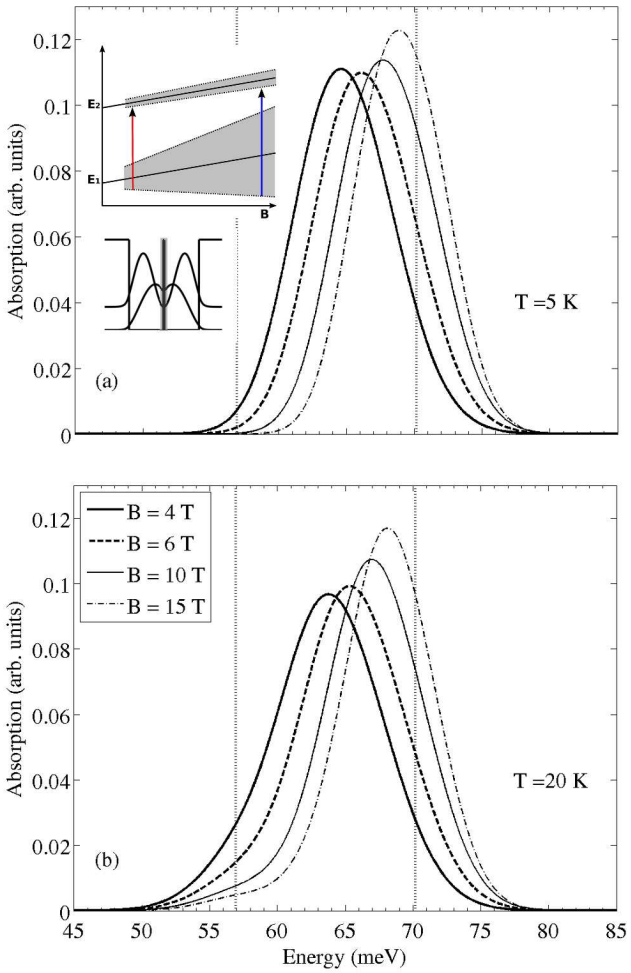

Figure 19. Calculated absorption spectrum of the DQW at different magnetic fields and (a) T=5 K and (b) 20 K. The upper inset panel in (a) depicts the field evolution of the independently broadened Landau levels. The ground Landau level is much broader than the excited one because of its larger probability of presence near the intermediate thin barrier. The arrow show that transitions involving correlated states at low T blueshift with increasing B.

and 6 meV respectively). Hence, these two in-plane electronic distributions look very different: the quasi E_1 state is extended in the (x, y) plane and its kinetic energy $\frac{\hbar^2 k^2}{2m^*}$ =3 meV is significantly larger than the characteristic potential depth. In contrast, the "mostly E_2 state" is fairly localized by the interface defects. In figure 21 we show the matrix $|\langle 1\nu|p_z|2\mu\rangle|^2$ for our calculated eigenstates of the disordered heterostructure. The figure clearly displays two blurred straight regions around $|E_2+\varepsilon_\mu-E_1-\varepsilon_\nu|$=73.8 meV, corresponding to the subband spacing in this sample if it were ideal. If there were no disorder, there would be no blurring since a single final state would match only one given initial state. The fact that the matrix element is almost zero if the energy difference between the true states differs strongly from the unperturbed inter-subband spacing corresponds well with the conventional broadening picture but hides an important

feature that is the taylorability of the inter-subband absorption width. It is interesting to note that the blurring is strongly reduced if the wave functions $\chi_n(z)$ for the E_1 and E_2 subbands are of the same magnitude at each interface $z{=}z_i$. Neglecting the inter-subband coupling due to interface roughness, nearly identical $\chi_n(z_i)$ provides very similar in-plane wavefunctions for both subbands, leading to a strong selection rules for the p_z-matrix elements as noted above in the large B analysis. Note that in the case of interface roughness this feature (nearly identical $\chi_n(z_i)$'s) is unlikely to happen because the penetration of the wavefunctions in the barrier increases with increasing subband energies.

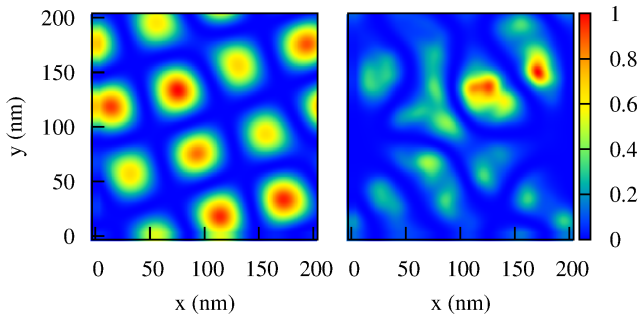

Figure 20. Color plot of the normalized in-plane probability distribution for two states with energies equal to $E_1{+}3$ meV (left panel) and $E_2{+}3$ meV (right panel). The quasi E_1 state is extended in the (x, y) plane while the quasi E_2 state is fairly localized by the interface defects.

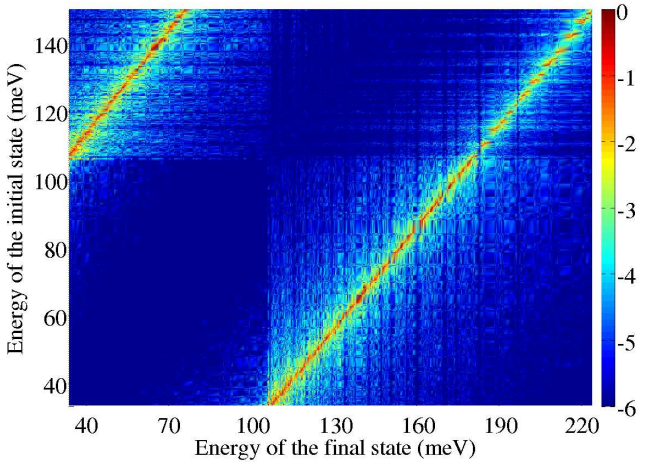

Figure 21. Color plot of the decimal logarithm of the normalized squared modulus of the optical matrix elements for the ensemble of transitions $E_2 - E_1 + \varepsilon_\mu - \varepsilon_\nu$ in a disordered 9/2/3 nm GaAs/$Ga_{0.75}Al_{0.25}$As DQW. The disorder is due to interface defects randomly distributed on the two inner interfaces of the structure.Reprinted with permission from [46]. Copyright 2012, American Institute of Physics.

The interface defects are relatively short ranged, are separable in $\vec{\rho}$ and z and produce shallow potential minima. Such is not the case of coulombic impurities

that display long tails, singularities and are not separable in $\vec{\rho}$ and z. The inter-subband absorption in superlattices in the presence of impurities has been calculated and measured [52–54]. The most striking feature of these absorption experiments and calculations is the existence of two absorption peaks corresponding respectively to transitions between the 3D extended states and to transitions between the bound or the quasi bound states attached to the two superlattice subbands. Similar results were obtained in QW structures [54]. In the case of heterostructures with low carrier concentration, we expect the binding energies of these bound or quasi bound states to be significant. However, our ability to taylor not only the layer thicknesses but also the doping profile allows a great flexibility in the inter-subband absorption lineshape. Consider a dilute concentration of Coulombic scatterers on a plane z=z_0 ($n_{imp}a^{*2} \ll 1$, where n_{imp} is the areal concentration of Coulombic scatterers and a^* the effective Bohr radius) of an heterostructure. These impurities are screened by n_e mobile electrons where n_e=n_{imp}. Since we shall set T=100 K and n_{imp}=2.17×10^{10} cm^{-2}, one can use a 3D Debye screening to account for the screening effects [30, 55]. Except in the vicinity (within a^*) of the scatterers, there is $(\vec{\rho}-\vec{\rho}_j)^2 \gg (z-z_0)^2$ and the screened Coulomb potential reduces to $-\frac{e^2}{4\pi\varepsilon_0\varepsilon_r|\vec{\rho}-\vec{\rho_j}|}\exp\left(-Q_s|\vec{\rho}-\vec{\rho_j}|\right)$, where Q_s is given in (14). On the other hand, very close from the impurity center there is:

$$\langle n|V_{Coulomb}|n\rangle \approx -\frac{e^2}{4\pi\varepsilon_0\varepsilon_r}\chi_n^2(z_0)\ln\left(\frac{|\vec{\rho}-\vec{\rho_j}|}{a^*}\right) \tag{69}$$

We see readily that the short-range behaviour of the effective in-plane potential will be identical if the probability densities of the electrons are the same in either subbands. Under such a circumstance, one should expect the emergence of an optical quasi-selection rule as indeed confirmed by figure 22. In figure 22, we show the contour plot analogous to that of figure 21 for Coulombic impurities sitting on the plane z_0=3 nm from the left hand side interface of the wide well including inter-subband couplings. We note that the blurring effect is even smaller than that due to interface defects. To illustrate the taylorability of the inter-subband absorption lineshape, we show in figure 23 the inter-subband absorption versus photon energy at T=100 K. In this figure three impurity planes have been considered: z_0=3 nm, z_1=8.45 nm where the wavefunction amplitudes at z_1 are identical and z_2=12.3 nm that corresponds to the maximum of the χ_2 wavefunction. The unperturbed transition energy occurs at 73.8 meV. We see that the absorption line corresponding to z_1 is narrower than in the two other situations and comprises a single line while in the two other cases the line is a doublet and is definitely broader [55]. The doublet corresponds to transitions between extended states and transitions between bound states in complete analogy with what was found in superlattices [53] and QW's [54].

We have found numerically that the inclusion of inter-subband scattering very little affects the emergence of quasi-selection rules as long as the subband spacing remains larger than the effective potential depth. Figs. 24a,b show the calculated absorption line in two GaAs/$Ga_{0.75}Al_{0.25}$As DQW structures (9/2/3 nm and 9.5/3/8.5 nm respectively) that markedly differ in the unperturbed inter-subband transition energy (73.8 meV

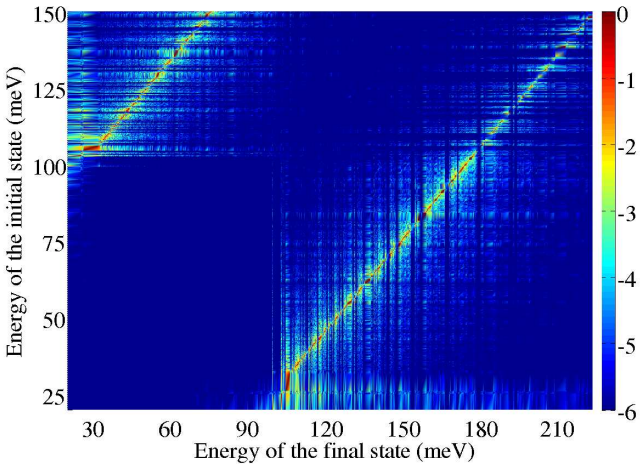

Figure 22. Color plot of the natural logarithm of the squared modulus of the optical matrix elements between the initial and final states of an optical transition in a disordered 9/2/3 nm GaAs/$Ga_{0.75}Al_{0.25}As$ DQW. The disorder is due to coulombic scatterers randomly distributed on the plane z_l=3 nm in the wide well. The areal concentration is 2.17×10^{10} cm^{-2}.

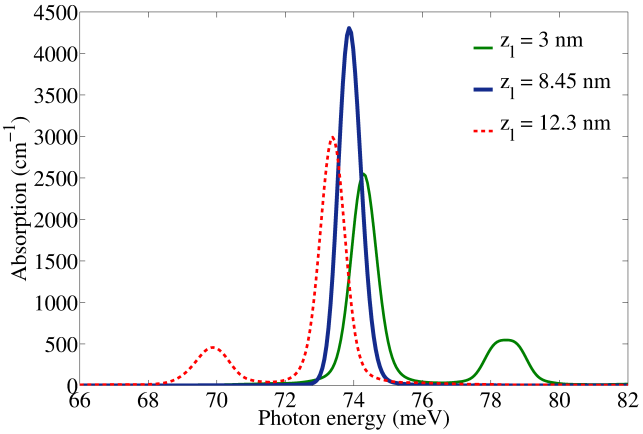

Figure 23. Calculated absorption spectrum of a 9/2/3 nm GaAs/$Ga_{0.75}Al_{0.25}As$ DQW in presence of coulombic impurities randomly distributed on a plane located at z_0=3 nm (blue dashed-dotted line), z_0=8.45 nm (green solid line) and z_0=12.3 nm (red dashed line). n_2=n_{imp}=2.17×10^{10} cm^{-2}. T=100K.[55]

and 7.3 meV respectively). For both structures there is a planar doping with an areal concentration of 2.17×10^{10} cm^{-2} located at the maximum of the wavefunction $\chi_2^2(z)$ of the second subband. The calculations have been done by either including (red solid lines) or excluding (blue dashed lines) inter-subband scattering [46]. It is seen that neglecting inter-subband scattering is a fair approximation in the large E_2-E_1 case while it gives a very poor description of the absorption lineshape in a case where E_2-E_1 is comparable to a typical binding energy. The increasing part played by inter-subband scattering in THz structures is a feature that strikingly constrasts with more conventional heterolayers.

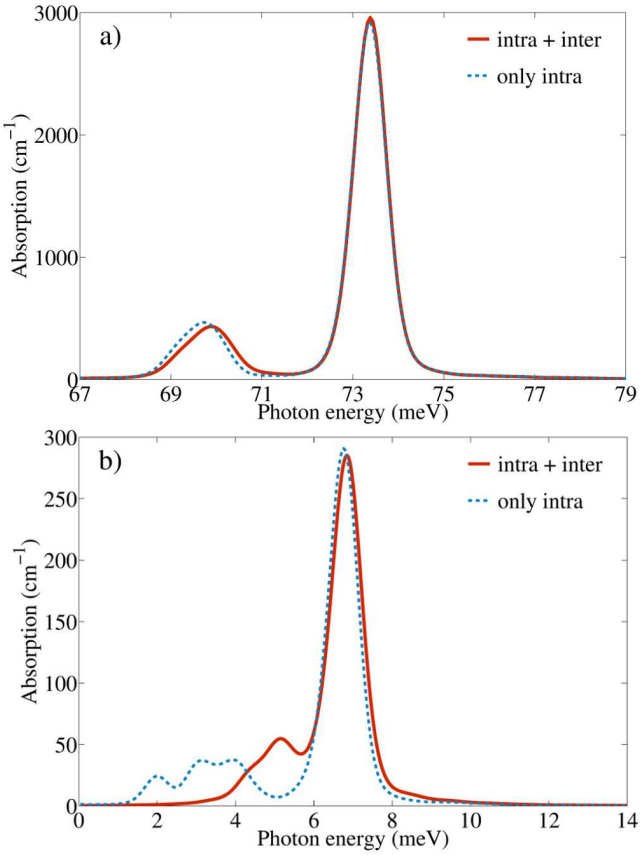

Figure 24. Calculated absorption spectrum of a 9/2/3 nm (panel a) and a 9.5/3/8.5 (panel b) GaAs/$Ga_{0.75}Al_{0.25}As$ DQW in presence of coulombic impurities randomly distributed on a plane located at the maximum of χ_2^2. The calculations have been done by either including (red solid lines) or excluding (blue dashed lines) inter-subband scattering. n_2=n_{imp}=2.17×10^{10} cm^{-2}. T=100K.

4. Conclusion

The low frequency Free Carrier Absorption in semiconductor heterostructures has a unique feature compared to FCA in bulk materials which is that it corresponds to doubly forbidden optical transitions associated with translation invariance and polarization selection rules for light propagating in the layer plane. Such oblique transitions become however possible in real structures, where the translational symmetry is broken due to impurities, interface roughness, etc. This leads to a weak FCA, considerably weaker than what could derive from an (incorrect) application of the Drude model. We have discussed the parts played by elastic (impurities, alloy scattering, interface defect) and inelastic (optical phonons) scatterers. We found that the interface defects in GaAs-based materials are not prevalent over other mechanisms but can become dominant in materials with non common anions such as (Ga,In)As/Ga(As,Sb). FCA can be evaluated in different ways and we have discussed Green's function techniques and perturbative approaches. The link between FCA and the tail of inter-subband absorption has been highlighted and we have thoroughly discussed which mechanisms control the absorption

line center and its wings. Finally, the role of dopant location has been stressed and we have established that one can control at will the lineshape of inter-subband absorption by a judicious placement of the dopants.

Acknowledgments

G. B. thanks the Technical University Vienna for hospitality. Discussions with G. Strasser and K. Unterrainer are gratefully acknowledged. The work at Lund University has been supported by the Swedish Research Council.

References

[1] Dumke W P 1961 *Phys. Rev.* **124**(6) 1813–1817
[2] Walukiewicz W, Lagowski L, Jastrzebski L, Lichtensteiger M and Gatos H C 1979 *J. Appl. Phys.* **50** 899–908
[3] Ando T, Fowler A B and Stern F 1982 *Rev. Mod. Phys.* **54**(2) 437–672
[4] Adamska H and Spector H N 1984 *Journal of Applied Physics* **56** 1123–1127
[5] Haug A 1992 *Semiconductor Science and Technology* **7** 373
[6] Yu P Y and Cardona M 1999 *Fundamentals of Semiconductors* (Berlin: Springer-Verlag)
[7] Vurgaftman I and Meyer J R 1999 *Phys. Rev. B* **60**(20) 14294–14301
[8] Liu H C and Capasso F 2000 *Intersubband Transitions in Quantum Wells: Physics and Device Applications I* (*Semiconductors and Semimetals* vol 62) (San Diego: Academic Press)
[9] Liu H C and Capasso F 2000 *Intersubband Transitions in Quantum Wells: Physics and Device Applications II* (*Semiconductors and Semimetals* vol 66) (San Diego: Academic Press)
[10] Haug H and Koch S 2004 *Quantum theory of the optical and electronic properties of semiconductors* (Singapore: World Scientific)
[11] Wacker A, Bastard G, Carosella F, Ferreira R and Dupont E 2011 *Phys. Rev. B* **84**(20) 205319
[12] Tsao J Y 1993 *Material Fundamentals of Molecular Beam Epitaxy* (Boston: Academic Press)
[13] Razeghi M 2011 *The MOCVD Challenge: A survey of GaInAsP-InP and GaInAsP-GaAs for photonic and electronic device applications* (New York: CRC Press)
[14] Gornik E and Tsui D C 1976 *Phys. Rev. Lett.* **37**(21) 1425–1428
[15] Ando T 1977 *J. Phys. Soc. Japan* **43** 1616–1626
[16] Kazarinov R F and Suris R A 1971 *Sov. Phys. Semicond.* **5** 505
[17] West L C and Eglash S J 1985 *Appl. Phys. Lett.* **46** 1156–1158
[18] Helm M, England P, Colas E, DeRosa F and Allen S J 1989 *Phys. Rev. Lett.* **63**(1) 74–77
[19] 1999 (*Semiconductors and Semimetals* vol 62) ed Liu H and Capasso F (Elsevier) pp 1 – 99
[20] Faist J, Capasso F, Sivco D L, Hutchinson A, Sirtori C and Cho A Y 1994 *Science* **243** 553
[21] Wacker A 2012 *Nonlinear Laser Dynamics* ed Lüdge K (Berlin: Wiley-VCH)
[22] Faist J 2013 *Quantum Cascade Lasers* (Oxford: Oxford University Press)
[23] Levine B 1992 *Intersubband Transitions in Quantum Wells* (*NATO ASI Series* vol 288) ed Rosencher E, Vinter B and Levine B (Springer US) pp 43–55
[24] Bastard G, Brum J A and Ferreira R 1991 *Solid State Phys.* **44** 229
[25] BenDaniel D J and Duke C B 1966 *Phys. Rev.* **152**(2) 683–692
[26] Ridley B K 1988 *Quantum Processes in Semiconductors* (Oxford: Claredon Press)
[27] Carosella F, Ndebeka-Bandou C, Ferreira R, Dupont E, Unterrainer K, Strasser G, Wacker A and Bastard G 2012 *Phys. Rev. B* **85**(8) 085310
[28] Leuliet A, Vasanelli A, Wade A, Fedorov G, Smirnov D, Bastard G and Sirtori C 2006 *Phys. Rev. B* **73**(8) 085311
[29] Regnault N, Ferreira R and Bastard G 2007 *Phys. Rev. B* **76**(16) 165121

[30] Nelander R and Wacker A 2009 *J. Appl. Phys.* **106** 063115
[31] Sakaki H, Noda T, Hirakawa K, Tanaka M and Matsusue T 1987 *Appl. Phys. Lett.* **51** 1934–1936
[32] Khurgin J B 2008 *Appl. Phys. Lett.* **93** 091104
[33] Goodnick S M, Ferry D K, Wilmsen C W, Liliental Z, Fathy D and Krivanek O L 1985 *Phys. Rev. B* **32**(12) 8171–8186
[34] Feenstra R M, Collins D A, Ting D Z Y, Wang M W and McGill T C 1994 *Phys. Rev. Lett.* **72**(17) 2749–2752
[35] Lew A Y, Zuo S L, Yu E T and Miles R H 1998 *Phys. Rev. B* **57**(11) 6534–6539
[36] Matyas A, Lugli P and Jirauschek C 2013 *Applied Physics Letters* **102** 011101 (pages 4)
[37] Kumar S, Chan C W I, Hu Q and Reno J L 2009 *Appl. Phys. Lett.* **95** 141110
[38] Unuma T, Yoshita M, Noda T, Sakaki H and Akiyama H 2003 *J. Appl. Phys.* **93** 1586–1597
[39] Banit F, Lee S C, Knorr A and Wacker A 2005 *Appl. Phys. Lett.* **86** 041108
[40] Benveniste E, Vasanelli A, Delteil A, Devenson J, Teissier R, Baranov A, Andrews A M, Strasser G, Sagnes I and Sirtori C 2008 *Appl. Phys. Lett.* **93** 131108
[41] Wacker A, Lindskog M and Winge D 2013 *Selected Topics in Quantum Electronics, IEEE Journal of* **19** 1200611
[42] Wacker A 2002 *Phys. Rev. B.* **66** 085326
[43] Willenberg H, Döhler G H and Faist J 2003 *Phys. Rev. B* **67**(8) 085315
[44] Wacker A 2007 *Nature Physics* **3** 298
[45] Ando T 1985 *Journal of the Physical Society of Japan* **54** 2671
[46] Ndebeka-Bandou C, Carosella F, Ferreira R, Wacker A and Bastard G 2012 *Appl. Phys. Lett.* **101** 191104
[47] Tamosiunas V, Zobl R, Ulrich J, Unterrainer K, Colombelli R, Gmachl C, West K, Pfeiffer L and Capasso F 2003 *Appl. Phys. Lett.* **83** 3873–3875
[48] Scalari G, Walther C, Sirigu L, Sadowski M L, Beere H, Ritchie D, Hoyler N, Giovannini M and Faist J 2007 *Phys. Rev. B* **76**(11) 115305
[49] Wade A, Fedorov G, Smirnov D, Kumar S, Williams B S, Hu Q and Reno J L 2009 *Nature Photonics* **3** 41–45
[50] Jasnot F R, de Vaulchier L A, Guldner Y, Bastard G, Vasanelli A, Manquest C, Sirtori C, Beck M and Faist J 2012 *Applied Physics Letters* **100** 102103
[51] Carosella F, Ferreira R, Strasser G, Unterrainer K and Bastard G 2010 *Phys. Rev. B* **82**(3) 033307
[52] Metzner C, Hofmann M and Döhler G H 1998 *Phys. Rev. B* **58**(11) 7188–7196
[53] Stehr D, Metzner C, Helm M, Roch T and Strasser G 2005 *Phys. Rev. Lett.* **95**(25) 257401
[54] Antoni T, Carras M, Marcadet X, Vinter B and Berger V 2010 *Appl. Phys. Lett.* **97** 042102
[55] Ndebeka-Bandou C, Wacker A, Carosella F, Ferreira R and Bastard G 2013 *Appl. Phys. Express* **6** 094101